Microgap Structured Optical Sensor for Fast Label-free DNA Detection

Yunmiao Wang

Thesis submitted to the faculty of the Virginia Polytechnic Institute and State University
in partial fulfillment of the requirements for the degree of

Master of Science
In
Electrical Engineering

Anbo Wang Chair
Yong Xu
Kristie L Cooper

May 3, 2011
Blacksburg, Virginia

Keywords: Fiber Optic Biosensor, DNA Sequence Identification, Fabry-Perot Interferometer, Microprobe

Microgap Structured Optical Sensor for Fast Label-free DNA Detection

Yunmiao Wang

ABSTRACT

DNA detection technology has developed rapidly due to its extensive application in clinical diagnostics, bioengineering, environmental monitoring, and food science areas. Currently developed methods such as surface Plasmon resonance (SPR) methods, fluorescent dye labeled methods and electrochemical methods, usually have the problems of bulky size, high equipment cost and time-consuming algorithms, so limiting their application for in *vivo* detection. In this work, an intrinsic Fabry-Perot interferometric (IFPI) based DNA sensor is presented with the intrinsic advantages of small size, low cost and corrosion-tolerance. This sensor has experimentally demonstrated its high sensitivity and selectivity.

In theory, DNA detection is realized by interrogating the sensor's optical cavity length variation resulting from hybridization event. First, a microgap structure based IFPI sensor is fabricated with simple etching and splicing technology. Subsequently, considering the sugar phosphate backbone of DNA, layer-by-layer electrostatic self-assembly technique is adopted to attach the single strand capture DNA to the sensor endface. When the target DNA strand binds to the single-stranded DNA successfully, the optical cavity length of sensor will be increased. Finally, by demodulating the sensor spectrum, DNA hybridization event can be judged qualitatively.

This sensor can realize DNA detection without attached label, which save the experiment expense and time. Also the hybridization detection is finished within a few minutes. This quick response feature makes it more attractive in diagnose application. Since the

sensitivity and specificity are the most widely used statistics to describe a diagnostic test, so these characteristics are used to evaluate this biosensor. Experimental results demonstrate that this sensor has a sensitivity of 6nmol/ml and can identify a 2 bp mismatch. Since this sensor is optical fiber based, it has robust structure and small size (125μm). If extra etching process is applied to the sensor, the size can be further reduced. This promises the sensor potential application of in-cell detection. Further investigation can be focused on the nanofabrication of this DNA sensor, and this is very meaningful topic not only for diagnostic test but also in many other applications such as food industry, environment monitoring.

Acknowledgement

I would like to express my deepest gratitude to my academic and research advisor Dr. Anbo Wang for his continuous encouragement, guidance and support in helping me to conduct and complete this work. I thank him for offering me such a good opportunity to study and work in an excellent research group with so many talented people, for enlightening me when I encounter difficulties in my research, for being a guild and model in my life.

I would also like to extend my gratitude to my other committee members, Dr. Kristie L. Cooper and Dr. Yong Xu. Thank you for the valuable suggestions and support during the preparation of this thesis. I am truly indebted to Dr. Cooper, as my first project manager and foreign friend, who helped me a lot in technical writing, research details and report preparation. I would like to sincerely thank Dr. Xu for his patience and effort as my qualification exam chair. Thanks for your valuable courses, so I could gain a basic understanding of optics.

I also owe a lot of thanks to the staff and students of CPT. Thanks Ms. Debbie Collins for her sincere administrative support. Very special thanks go to Miss Dorothy Y. Wang and Mr. Cheng Ma. Thanks for your helpful discussions and valuable friendship. Thanks Dr. Ming Han, Dr. Evan Lally, Mr. Bo Dong, Dr. Yizheng Zhu, Dr. Zhuang Wang, Dr. Xingwei Wang for the knowledge and support.

Finally I want to express my deepest love to my parents. Thanks for your endless encouragement and support for me when I feel frustrated during the study.

Content

List of figures

List of Tables

Chapter 1 Introduction

1.1 Introduction to optical fiber sensors

Optical fibers, which emerged in the 1960s, can be used for a variety of sensing purposes, providing a measurement technology which presents advantages over conventional methods in several areas [1]. Optical fiber sensors have the characteristics of small size, low weight, immunity to electromagnetic interference, chemical passivity, the capabilities of dense multiplexing and remote measurement. Meanwhile the well-developed optical components and devices from the optical communication industry provide economic convenience to the optical sensor industry.

1.1.1 Classification of optical fiber sensors

Optical sensors can generally be classified into four categories based on light characterizing sensing parameters: intensity modulation, wavelength modulation, polarization modulation and phase modulation.

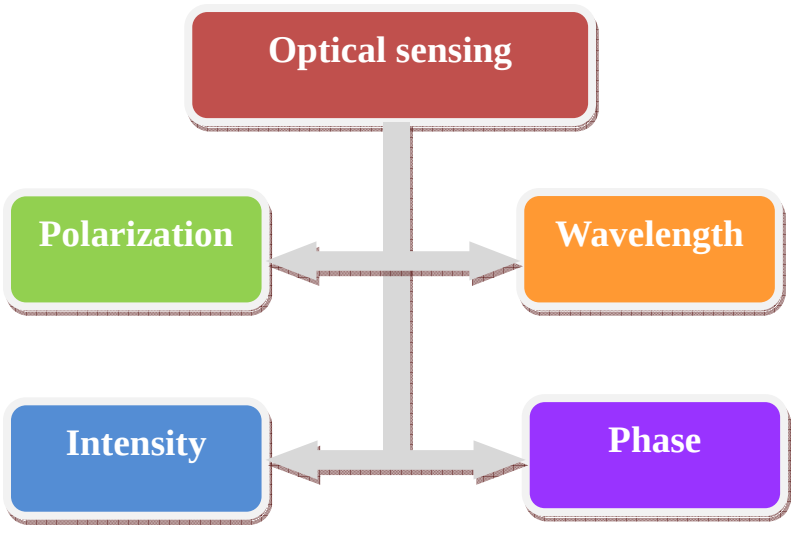

Figure 1.1 Categories of optical fiber sensors

Intensity modulation:

This method was employed in early optical sensor development and featured simplicity, reliability, and low cost [2]. The intensity of light launched into a sensor head from a light source varies in accordance with the measurand. The intensity modulated light is detected by a light receiving component and converted into an electrical signal. A change in the electrical signal is proportional to the change of the measurand. Various sensors, such as mass and electrical current sensors have been developed based on this modulation scheme [3, 4]. The main limitation of this method is the need of some power reference to avoid errors arising from source instability, variable losses in fibers and connectors.

Wavelength modulation:

Wavelength modulation is a form of modulation in which the wavelength shift of the optical sensor is changed by the measuring quantity. A broad bandwidth light source is used to interrogate the sensor and by comparing the amplitude shift at two (or several) fixed wavelengths or via continuous wavelength scanning, the wavelength shift is obtained. Typical optical sensors of this kind include fluorescence sensors and Bragg grating sensors. Fluorescence-based sensing has been demonstrated to be a significant technique in prominent fields such as fluorescence-activated cell sorting, DNA sequencing, high-throughput screening, and clinical diagnostics [5]. Fiber Bragg grating sensors are widely used for temperature and strain monitoring in some civil structures. However, in order to obtain good sensitivity, this configuration usually has requirements on the bandwidth of the light source and the resolution of the spectrometer, which will increase the system cost.

Polarization modulation:

The scheme realizes the measurement by detecting the change in the polarization of light introduced by the sample. The system typically consists of a linearly polarized light

source, a crossed analyzer formed from two orthogonal linear polarizers, and a detector. The amplitude of the detected signal depends on a change in the state of polarization introduced by the sample. This method has been utilized in biomedical sensing [6] and electrical or magnetic field measurement [7]. One drawback of polarization modulation is the possible error induced by random polarization change in the system such as the birefringence of optical fiber.

Phase modulation:

Phase modulation is the mechanism behind all interferometric sensors. In this scheme, the measurand causes a change in the phase of the detected signal, which is a cosine interference function. Interferometric sensors have been investigated for decades and exhibit advantages in some physical parameters with high sensitivity such as temperature, strain and pressure. Interferometric sensors include Sagnac, Mach-Zehnder, Michelson and Fabry-Perot interferometric sensors. Among these sensors, Fabry-Perot interferometric sensors are most widely applied [8].

1.2 Biological sensing

Biosensing technologies are of increasing importance in healthcare, food production and processing, environmental and security sectors. In a broad sense, the study of biosensing includes biological identification, electrical or photonic detection and the computer algorithms used to interpret data. It is a wide and multidisciplinary research field, spanning biochemistry, physical chemistry, electrochemistry, electronics and software engineering.

1.2.1 Definition

A biosensor is a probe that integrates a biological component, such as a whole bacterium or a biological product (for example: an enzyme or antibody) with an electronic

component to yield a measurable signal [9]. A biosensor consists of three basic elements: a bioreceptor, a transducer and a detector. The bioreceptor interacts with a specific target analyte and generates a physical or chemical change. This change will be further converted into a measurable optical or electrical signal by the transducer. A detector element is employed to read out the measurable signal. The identification mechanism between the bioreceptor and the analyte plays a key role in the sensitivity and selectivity of the sensing. An example of a biosensor is an optical fiber attached to an antibody that reacts specifically with the carcinogen benzopyrene (*BaP*) for the detection of the cancer-induced agents in groundwater [9]. The binding between the antibody and the *BaP* will produce fluorescence, which can be guided by the optical fiber and measured.

There are several primary requirements for successful biosensors:

1. The bioreceptor must be highly specific for the analyte under the normal conditions.
2. The detection should be accurate, reproducible and linear with the concentration of the analytes.
3. The complete biosensor should be compact, economic, portable and immune to environmental noise.
4. For invasive diagnosis, the bioprobe must be tiny, biocompatible and free of antigenic effects.

1.2.2 Sensing method

Depending on the operating principle of transducers, biosensors can be classified into electrochemical, piezoelectric, and photometric varieties as shown in Figure 1.2.

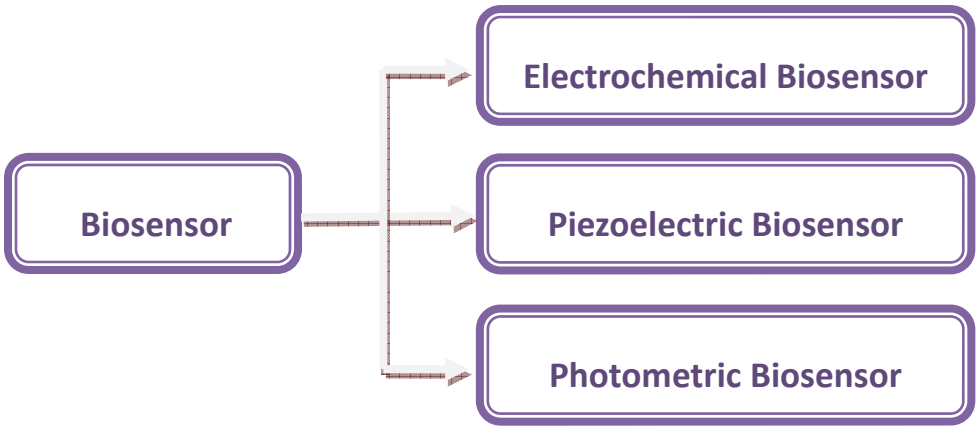

Figure 1.2 Classification of biosensors

Electrochemical biosensor

An electrochemical biosensor is a biosensor with an electrochemical transducer. The enzyme in the bioreceptor has an electro-active substance, and the reaction between the enzyme and the analyte can be transferred into a measurable electric signal, which is proportional to the analyte concentration. There are three common methods to convert chemical information into a measurable electric signal: amperometry, potentiometry, and conductometry. Amperometry measures the resulting current due to the reduction of an electroactive enzyme or electrochemical oxidation. Potentiometry is based on the potential difference between two reference electrodes separated by a permselective membrane. The electrodes can be ion-sensitive electrodes (ISE) or ion-sensitive field effect transistors (ISIFET) and the signal is produced by the ions accumulated at the ion-selective membrane due to changes occurring at the surface of the bioreceptor [10, 11]. Conductometry uses conductometric or impedimetric devices to monitor enzyme reactions. To achieve high sensitivity, a differential conductance measurement is usually performed between a sensor with enzymes and an identical one without enzymes [10]. Since Leland C. Clark proposed the principle of the first enzyme electrode with immobilized glucose oxidize in 1962 [11], electrochemical biosensors have been

developing rapidly for nearly fifty years, and many commercialized devices based on this principle have been proposed. One such is a glucose sensor for diabetics.

Piezoelectric biosensors

Piezoelectric biosensors utilize the piezoelectric effect of some crystals, which have a physical deformation that is proportional to an applied electrical potential. When acoustic waves, which can be viewed as a standing wave, propagate through the crystal, the characteristic frequency of acoustic waves can be modulated by the piezoelectric properties of the crystal. If a biological recognition element is coated on the surface of such a crystal, the reaction between the analyte and the bioreceptor can change the piezoelectric properties of crystal, and this change can be subsequently interpreted by monitoring the frequency of acoustic waves. Many types of crystals exhibit the piezoelectric effect, but the electrical, mechanical, and chemical properties of quartz make it the most common crystal type used in biosensing applications [12]. Biosensors based on piezoelectric quartz crystal have been widely investigated and several applications are reported including DNA hybridization, enzyme detections and gas phase biosensors [13-15]. The advantages of piezoelectric biosensors include high sensitivity and specificity, rapid response time and reduced influence of interferences. The primary problems with piezoelectric sensors are the lack of an exact correlation between mass addition and frequency change for solution phase sensing, and the sensitivity to environmental conditions [12].

Optical biosensors

Optical biosensors are based on different optical phenomena, including fluorescence, luminescence, absorption, interferometry, evanescent wave and surface plasmon resonance, to convert biological information into the measurable optical signal. In this section, the basic principles of several major phenomena will be introduced briefly.

Fluorescence is a commonly used phenomenon in optical biosensors. Fluorescence is the re-emission of a wavelength by molecules which have absorbed the radiation of a specific different wavelength. For each molecule, the fluorescence spectrum is characteristic and thus can be used to identify a particular molecule. In a fluorescence-based optical biosensor, a fluorescent-labeled antibody (sensing element) is attached to the end of an optical fiber, which is used to transmit the excitation light. The sensing is achieved by monitoring the fluorescence intensity, which is proportional to the bonding between the antigens (analyte) with the antibody.

Absorption is a simple phenomenon used in biosensing. Absorption is a process in which the energy of a photon is transformed to other forms of energy, such as heat. The absorbance of a molecule at a specific wavelength can be used to determine the concentration according to Beer-Lambert law. A common configuration to measure the absorbance is to direct a beam of radiation at the sample and detect the intensity of the radiation that passes through it. Some absorption spectroscopy techniques that have been developed to measure the absorption as a function of wavelength include ultraviolet-visible spectroscopy, infrared spectroscopy, and X-ray absorption spectroscopy.

Surface plasmon resonance (SPR) is another phenomenon used in optical biosensing. SPR describes the optical excitation of surface plasmons, which are surface electromagnetic waves that propagate on the boundary between a metal and an external dielectric (gas, liquid or solid) [16]. To realize the optical excitation of surface plasmons, a thin metal film will be evaporated onto a planar waveguide. When light propagating in the waveguide, evanescent waves penetrate the metal film, and plasmons will be excited on the outer side of the film. Since the metal absorbs the energy from

the light in this process, there will be a narrow dip in the reflection spectrum. SPR is extremely sensitive to the change in refractive index at the boundary of metal. Many configurations have been developed to realize SPR, such as the Kretschmann prism configuration [16] and the grating scheme [17].

1.2.3 Biomedical application of optical fiber sensors

One large field of optical fiber sensor applications is clinical and biochemical sensing [18]. The intrinsic features of optical fiber sensor make it more attractive in biomedical applications compared with some traditional methods. The important aspects are summarized as below:

1. The miniature size potential afforded by micro or nano fabrication techniques. The size of ordinary optical single mode fiber is 125μm, which can be further reduced by micro or nano silica fabrication techniques. This will make them more useful in some cases of small sample volume or invasive diagnosis.
2. Immunity to electrical signal. Considering the static electricity of the body, the optical fiber sensors are more competitive than electrical sensors which can suffer from electrical interference.
3. Capability of simultaneously monitoring multiple analytes. If one optical fiber sensor is modified for one specific analyte, a bundle of optical sensors with different modified outlayers on the sensor heads can be used to simultaneously detect various samples such as pH, blood sugar and oxygen without cross-sensing.

In the past decades, the optical fiber sensor has been successfully used for several biomedical applications such as body temperature, blood pressure, pH, and antibody measurements. One elegant example is a temperature sensor designed by ASEA [18], which can realize 0.1℃ resolution over the 0 to 200℃ temperature range.

Additionally, researchers have developed various optical fiber sensors for pH, blood pressure, and some gas concentrations such as oxygen and CO [19-21], which are important for a correct and effective diagnosis of a disease. Furthermore, by exploiting the interaction of antibodies with antigens, an antibody optical fiber sensor has been realized by attaching a specific antibody on a fiber end with surface modification techniques.

1.3 Motivation of DNA detection

Sequence-specific DNA detection in real time and with high sensitivity is of great scientific and economic interest in medical diagnostics, pathology, food safety, and other fields. The investigation of DNA interaction has profound implications for our understanding of cellular processes and disease mechanisms such as cancer. Some DNA biosensors have been developed but they are associated with problems such as long assay time, bulky size and additional reagent preparation. The motivation behind improving DNA sensing is to develop a compact and economic sensor to realize a fast, simple, and reliable DNA detection.

UV spectroscopy is a classic method which works well for a pure sample of nucleic acids but suffers the cross-contamination from proteins, which also have the absorption peak in the same wavelength range [22]. Another well-established method is a fluorescence measurement relying on a cationic organic dye attached to DNA. The attachment of the necessary labels not only increases the testing time and requires highly trained personnel, but also increases the risk of contamination and mechanical damage to the probe, and may perturb the conformation of the DNA probe. Besides, the external illuminator used to excite the fluorescence collected by the fiber makes the whole system bulky and

expensive [23]. Polymerase chain reaction (PCR) is a nucleic acid amplification method that has improved the sensitivity and specificity of DNA test. This method involves repeating 3 basic steps: denature target strands, anneal primers, and amplify the strands. Thus it typically takes a long time to acquire the data [24].

Compared to spectroscopic methods, fluorescent probes and PCR methods, optical fiber sensors have the intrinsic advantages of small size, low cost and ease of use. The material of optical fiber also makes it a suitable candidate as a biosensor. Silicon dioxide, due to its durability can be used in harsh environments or be incorporated with DNA by a surface modification technique based on chemical or electrical bonding [25]. Another attractive feature of the optical fiber probe is the feasibility of further reduction of size by pulling or etching methods [26, 27]. Such sensors hold a great potential for intracellular monitoring, which will revolutionize the fundamental approaches in cell biology.

1.4 Research motivation and thesis organization

Xingwei Wang et al. at Virginia Tech's CPT previously proposed and demonstrated a fiber Fabry-Perot interferometric sensor for label-free DNA sequence detection [28]. In this previous work, the sensor consists of a hollow optical fiber spliced to two singlemode fibers. It is thus difficult to further reduce the sensor size simply by the traditional fiber tapering or etching methods. Moreover, the reproducibility of this hollow core fiber based Fabry-Perot cavity is difficult to control. The goal of this research is to develop a label-free and robust optical fiber probe that can specifically detect a target DNA sequence with improved sensor simplicity and fabrication reproducibility. More importantly the sensor has the potential to significantly reduce its size for applications, such as in-cell detection of DNA, where small size is essential.

This thesis is organized as follows:

Chapter 2 describes the design of a microgap structure optical fiber sensor, including the principle of Fabry-Perot interferometery, the fabrication of the actual sensor head, and the interrogation system.

Chapter 3 presents the layer-by-layer electrostatic self-assembly technique for the sensor surface modification. The experiment for the measurement of the thickness of multiple layers deposited on the sensor end face is described.

Chapter 4 introduces the DNA immobilization and hybridization experiment and presents the investigation of the sensor sensitivity and the selectivity.

Chapter 5 summarizes the contribution of this work and discusses the potential improvement for future research.

Chapter 2 Sensor principle and measurement system

2.1 Fabry-Perot Interferometer Theory

Optical sensing technology arose in the early 1970s as a result of the success of some low-loss optical fiber experiments [1]. In recent days, this field has developed to include a range of diverse technologies which are becoming more competitive in various applications compared with conventional methods. In optical fiber sensing, the major technologies include fiber gratings, interferometers, luminescence, and others. The Fiber optic Fabry-Perot interferometer (FFPI) was produced by introducing mirror coatings on a fiber. As an interferometer, the FFPI inherits the advantages such as high sensitivity, ease of fabrication, and location insensitivity. Based on the interference fringe, the Fabry –Perot cavity length can be deduced. Since environmental parameters such as temperature, pressure, and others can influence the Fabry-Perot cavity, their sensing can be realized by measuring the cavity length change. With white-light interferometry, FFPI sensors can achieve high resolution and large dynamic range together with absolute measurement [29].

2.1.1 Geometrical theory of Fabry-Perot structure

A Fabry-Perot interferometer typically consists of two reflecting surfaces separated by a transparent plate as shown in Figure 2.1. When a plane wave of monochromatic light is incident up on a Fabry-Perot cavity, interference is caused by the multiple reflections of light between the two reflecting surfaces. The peaks and valleys of the interference pattern correspond to constructive interference and destructive interference respectively. For a low-finesse Fabry-Perot interferometer, it could be approximated as two beam

interference. The total reflecting light intensity I can be expressed as:

$$I = I_1 + I_2 + 2\sqrt{I_1 I_2}\cos(\frac{4\pi nd}{\lambda} + \phi_0) \qquad 2.1$$

I_1, I_2 : intensities of the two reflecting beams

λ : light wavelength in vacuum

d : Fabry-Perot cavity physical length

n : refractive index of the cavity

ϕ_0 : initial phase shift

From this equation, it is clearly shown that the output intensity varies with the differential phase delay between the two reflections, which can be designed to be related to parameters of our measurement interest.

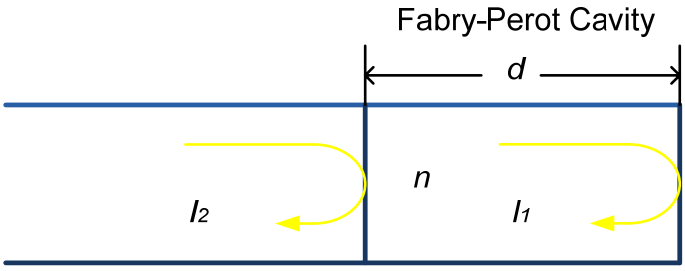

Figure 2.1 Illustration of Fabry-Perot interferometer

2.1.2 Classification of Fabry-Perot sensor

According to the structure of the cavity, a Fabry-Perot sensor can be classified as either an extrinsic Fabry-Perot interferometer (EFPI) or an intrinsic Fabry-Perot interferometer (IFPI). The cavity of an EFPI is formed outside the fiber usually by an air gap between two fiber ends, and the fibers are connected by a tube with an inside diameter slightly larger than the fiber diameter. UV glue and epoxy resin can be used to connect the tube and the

fiber. The quality of the connect points decides the physical continuity and the mechanical robustness. The interfaces between the fiber and air serve as two reflectors as shown Figure 2.2a. EFPIs are now widely applied in various sensing area including strain. A drawback of EFPI sensors is that they must be calibrated and, in some designs, they measure only relative strain and therefore cannot tolerate power interruptions [1].

In IFPI sensors, the cavity is built within the fiber as shown in Figure 2.2b and the cavity length is defined as the distance between the two reflectors. The reflector is essentially realized by the different reflective index contrast and several methods can be applied to fabricate the local reflectors such as dielectric thin-films [30], fiber Bragg gratings [31] or UV-induced mirrors [32]. Since the optical fiber is the cavity material, an IFPI can be used as a temperature sensor due to the temperature sensitivity of fiber. In addition, IFPIs have experienced success in fiber optics communication as in-line tunable filters in WDM systems [33-35].

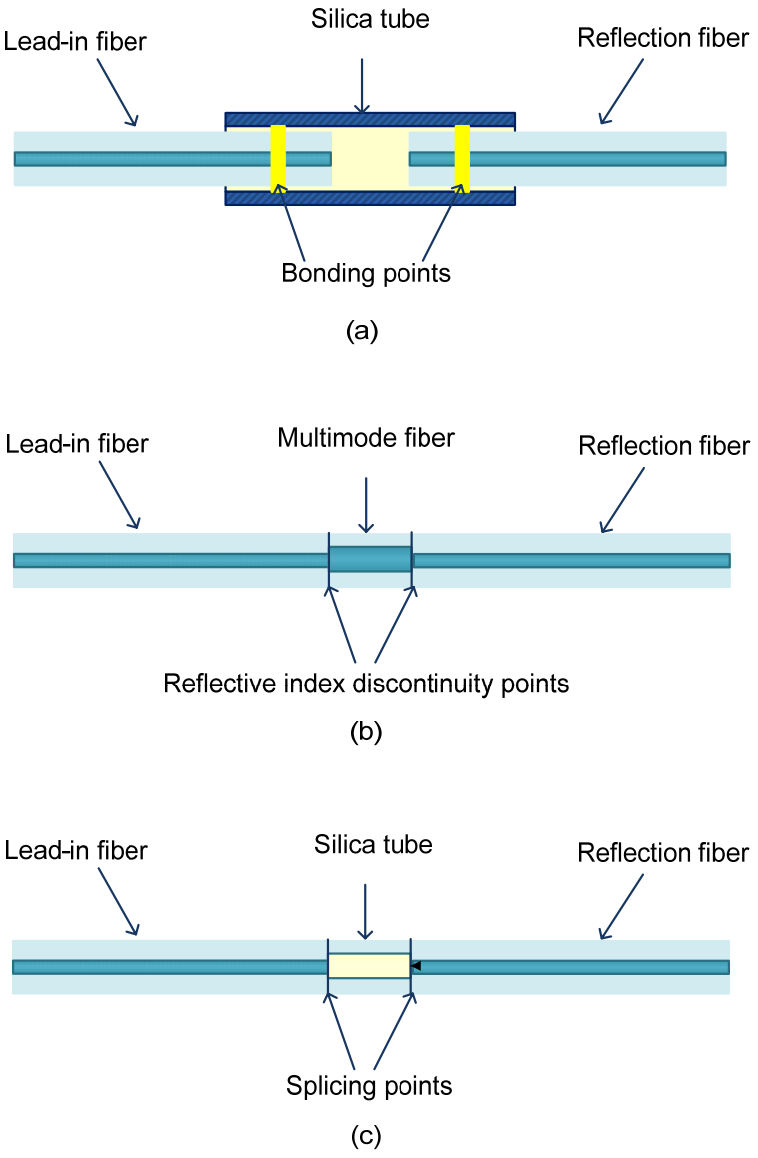

Figure 2.2 Classification of Fabry-Perot interferometer (a) EFPI sensor fabricated by laser bonding (b) IFBG sensor formed by single mode and multimode fibers. (c) ILFPI sensor fabricated by splicing.

An In-line Fabry-Perot interferometer (ILFPI) is a hybrid of EFPI and IFPI, as illustrated in Figure 2.2c. A cavity is formed between two fiber end-faces by splicing them to a section of hollow-core fiber of the same outer diameter as the fiber. Using the splicing method reduces the outer diameter size of the ILPI and also ensures a smooth profile compared with an EFPI. An ILPI can also be fabricated by etching method. A cavity can be sealed

by splicing a properly etched fiber with a well-cleaved single fiber. In this method, the etching process should be carefully designed to achieve an ideal size.

2.1.3 Application of Fabry-Perot sensors

As one of the major fiber sensor technologies, fiber Fabry-Perot interferometric (FFPI) sensors have been widely used in temperature, pressure and chemical measurements [36-44]. This kind of sensors possess a series of characteristics such as compactness, lightweight, and generally immunity to electromagnetic interference (EMI)[1].

One application is temperature monitoring in such industries as automation and aerospace. As early as 1970, optical sensor attracted many researchers to temperature sensing. Due to characteristics of the material SiO_2, the optical sensor can usually be used in high temperature testing and the sensing is done by measuring the temperature induced reflective index variation. It was reported that a Fabry-Perot based on optical fiber can be operated as high as 600 ℃ [45], which is a dramatic improvement compared with traditional semiconductor-based temperature sensors, which have the maximum limit of 500℃. Combined with the material sapphire, the Fabry-Perot temperature sensor has the potential to challenge higher temperatures.

Pressure sensing is another major application of Fabry-Perot interferometers. This application is demanded in both the industrial community and invasive medical systems. For example, pressure testing in harsh environment such as jet engines or power generation systems will prefer robust and stable sensors. Traditional electrical-based sensors can not meet these requirements due to inherent problems including bulky size, strong temperature dependence and long time instability. Fabry-Perot optical sensors can be designed to adapt to corrosive conditions since it is capable of high operating temperatures, chemical

inertness, and low cost. Besides, the trend of miniaturizing medical instrumentation makes this sensor an attractive candidate for the diagnosis applications. One example is continuous monitoring of the intracranial pressure of head trauma patients by fiber-optic catheters tipped with a small displacement diaphragm in front of two fibers, which form a Fabry-Perot interferometer [7].

Fabry-Perot interferometers can also be utilized as chemical sensors. The general scheme for chemical sensing is attaching a reagent to the end of the sensor. The chemical reaction between the species and the reagent will be measured by monitoring the cavity change. Chemical sensing can be applied to underwater and soil contamination monitoring.

2.2 Structure of Microgap Sensor

2.2.1 Introduction

Microgap sensors are a kind of IFPI featuring an air gap sealed by two spliced single mode fibers. As discussed early, FFPIs can be classified into EFPIs and IFPIs. EFPIs are employed in some sensing areas; however, this kind of sensor is limited by some intrinsic problems such as bonding difficulty and the discontinuity of diameter. IFPIs contain the cavity inside the fiber and usually have continuous geometry and robust structures compared with EFPI. Many methods are employed to fabricate an IFPI. As mentioned previously, the local reflectors or mirrors inside the fiber can be formed by dielectric thin films [30], fiber Bragg gratings (FBG) [31], and UV-induced mirrors [32]. Dielectric mirrors can be deposited onto the fiber by magnetron sputtering, and can achieve 85% reflectance [30]. At the same time, problems such as the deterioration in film quality during splicing limit this method. FBG is another commonly used technique to form the mirror within an optical fiber [46]. Also the internal reflector can be realized by splicing

two fibers with different reflective indices [47], for example: single mode fiber (SMF) and multimode fiber (MMF). This method eliminates the problem of poor joint-point quality. Usually SMF and MMF have different core size, so when light travels from SMF to MMF, higher order modes are generated which subsequently leads to more difficult signal decoding.

For microgap sensors, a microgap formed by a well-cleaved fiber and an etched fiber serves as one internal reflector. The other end of the etched fiber is the second reflector and the cavity length is defined by these two reflectors. This cavity is used as the transducer, whose length increases when the sensor head is deposited with polymers which then immobilize DNA. By decoding the interference fringe, the cavity length can be calculated with high accuracy and resolution. The fabrication of such a microgap sensor involves fiber etching and splicing. These processes are simple, low-cost, and suitable for batch production. This structure inherits the advantages of IFPIs such as small size, robustness and profile straightness, and at the same time it excels with the potential to be etched to nanometers. This will be very meaningful for in-cell DNA detection.

As introduced early, the total interference fringe can be expressed as Equation 2.1 and ignoring the constant component (I_1+I_2), the fringe varies as a cosine function. The fringe visibility is a very important parameter and is defined as:

$$V_b = \frac{I_{\max} - I_{\min}}{I_{\max} + I_{\min}} \qquad 2.2$$

Here I_{max}, and I_{min} are the maximum and minimum intensities in the interference spectrum respectively. Since the fringe visibility largely determines the system signal-to-noise ratio (SNR), the fringe visibility should be considered during the sensor design.

If light enters the Fabry-Perot cavity with an incidence angle Θ, as shown in Figure 2.3, n_1 is the reflective index of the upper surrounding medium; n_2 is the reflective index of the cavity material and n_3 is the reflective index of the lower surrounding medium. The reflection coefficient and transmission coefficient for the first reflector (from n_1 to n_2) are r and t; the reflection coefficient and transmission coefficient for the second reflector (from n_2 to n_3) are r' and t'. Assuming no surface absorption and transmission loss, the magnitude of the *mth* reflected beam can be written as

$$A_m = t \times t' \times r^m \times r'^m \times E_i \qquad 2.3$$

Here E_i is the magnitude of incident light, and the phase delay between two adjacent reflections is

$$\phi = 4\pi \times n_2 \times d \times \frac{\cos\theta'}{\lambda} \qquad 2.4$$

The amplitude of the total reflected electric field E_r can be derived from Equations 2.3 and 2.4 as

$$E_r = \sum_{m=0}^{\infty} A_m \exp[-j(m+1)\phi] \qquad 2.5$$

The intensity of reflected light can thus be written as

$$I_r = E \cdot E^* = \frac{4R\sin^2(\frac{1}{2}\phi)}{(1-R)^2 + 4R\sin^2(\frac{1}{2}\phi)} \times I_i \qquad 2.6$$

Here I_i is the intensity of the incident light and $R = r \times r'$. According to Equation 2.6, the reflection spectrum of the Fabry-Perot interferometer is clearly a function of wavelength. Figure 2.4 shows the simulation of Fabry-Perot spectra with different R values. Obviously higher R gives rise to sharper fringes, which correspond to a higher fringe visibility. For light with near-normal incidence to the interface ($\Theta=0$), the reflection coefficients of the first and the second reflectors are given by :

$$r = \frac{(n_1 - n_2)^2}{(n_1 + n_2)^2} \qquad 2.7$$

$$r' = \frac{(n_2 - n_3)^2}{(n_2 + n_3)^2} \qquad 2.8$$

Since $R = r \times r'$ which affects the fringe visibility, the fringe visibility is related to the reflective index contrast for each mirror $\Delta n = n_i - n_{i+1}$. Here n_i and n_{i+1} are the reflective indices of the materials surrounding the mirror.

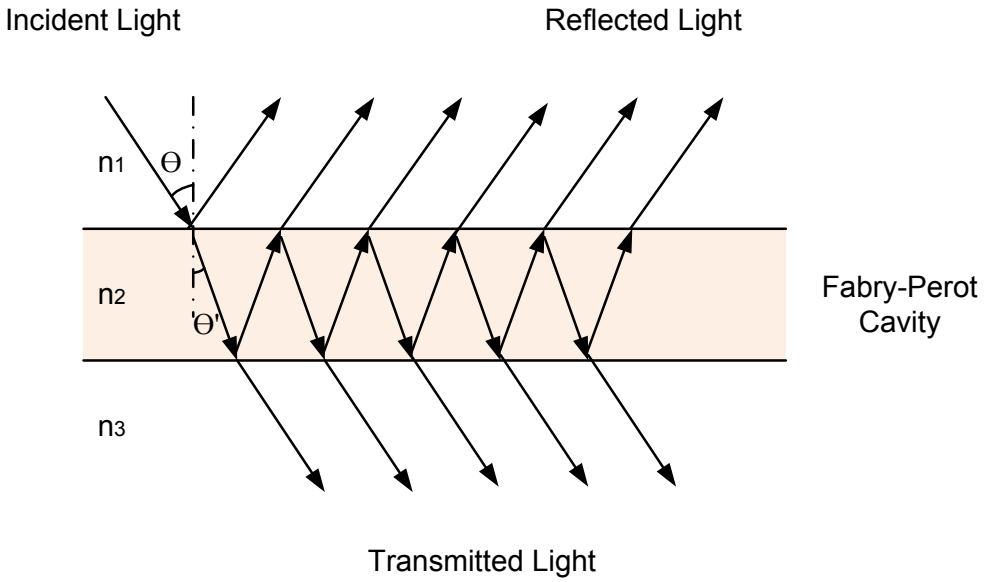

Figure 2.3 Fabry-Perot cavity interference model

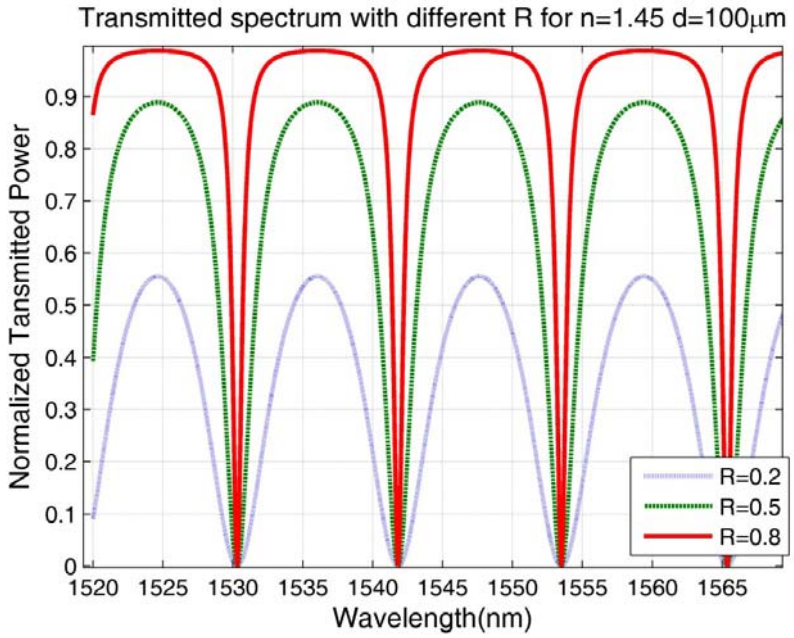

Figure 2.4 Transmission spectra for a Fabry-Perot cavity with different R

The concept of the microgap structure sensor as a DNA detection sensor comes from two considerations. As introduced earlier, many methods such as the electrochemical method [48], surface plasma method [49] and fluorescent dye-attached method [50] have been proposed as a scheme to fabricate DNA sensors. However, all of these methods are limited by the size problem and the fact that they cannot realize in *vivo* examination. The optical fiber biosensor has the intrinsic advantage of small size. To further achieve in-cell target detection, the size of optical fiber should be reduced to nanoscale sizes through extra processes such as tapering and etching. Considering the requirement for subsequent etching or tapering treatment, the initial structure of the sensor should be robust and reliable in order to endure this treatment, while at the same time maintaining the sensing functionality. In this case, FBG and dielectric film deposition are excluded because the functionalized structure will disappear after the subsequent method for sensor fabrication. In contrast, the etch-induced air gap of a microgap structure is usually 1-2 microns and well sealed in the central core area. This means that during the etching or pulling process, the

lateral size of the cavity may be reduced, but the quality of two reflectors will be influenced at a minimum level. On the other hand, the fringe visibility, which largely determines the system SNR, has to be considered. For example, the internal mirror can be fabricated by splicing two fibers like single mode fiber (SMF) and multimode fiber (MMF) with different refractive indices. Such a structure can also survive the following size reduction process. However, this kind of sensor shows a low fringe contrast compared with a microgap sensor as the sensor is downsized [28]. When light travels from a SMF to a MMF, the reflection coefficient from the joint of the two fibers may be approximately expressed as

$$r \approx \frac{(n_{core-MMF} - n_{core-SMF})^2}{(n_{core-MMF} + n_{core-SMF})^2} \qquad 2.9$$

For a graded index multimode fiber (Corning Infinicor, Δ=1%, a=25μm) and a single-mode fiber (Corning SMF28, Δ=0.32%, MFD=4.2 μm), the reflection coefficient can be roughly estimated to be $r \approx 1.17 \times 10^{-3}\%$. However if the microgap is used as the internal mirror, the reflective coefficient for this mirror can be approximated as

$$r = 2 \times \frac{(n_{core-SMF} - n_{air})^2}{(n_{core-SMF} + n_{air})^2} \approx 2 \times \frac{(1.45-1)^2}{(1.45+1)^2} = 6.74\% \qquad 2.10$$

The reflection coefficients *r'* of the second mirror for these two structures are almost the same. Thus $R = r \times r'$ is mostly determined by the internal mirror reflective coefficient *r*. Based on the previous analysis, a higher *R* yields to sharper fringes. Comparing the *R* values for these two structures, the conclusion is that microgap structure yields a better fringe visibility.

2.2.2 Fabrication

The fabrication of the microgap structure includes three major processes: first etching the core of a single mode fiber (SMF) from its end into the fiber slightly; secondly splicing this

etched fiber to another well-cleaved leading SMF and finally cleaving the other end of the etched SMF to form the Fabry-Perot cavity.

Chemical etching is a commonly used technique in optical fabrication, such as nanoprobes [51], and microwells [52] . The general idea is to use hydrofluoric acid (*HF*) to etch the fiber tip. The advantage of this method is that the profile of the fiber head can be adjusted by changing the etching solution. This method is also easy to operate and inexpensive. At the same time, since *HF* is a kind of toxic acid and will do harm to people's health, the etching process should be finished in a fume hood by trained people.

When a fiber is dipped into a solution of hydrofluoric acid (*HF*) and ammonium fluoride (NH_4F) buffer, the core and the cladding of single mode fiber (Corning, SMF28) have different etching rates because the core area is germanium-doped silica and the cladding is pure silica. The reaction process can be described as [53]:

$$SiO_2 + 4HF + 2NH_4F \rightarrow (NH_4)_2 SiF_6 + 2H_2O \qquad 2.11$$

$$GeO_2 + 4HF + 2NH_4F \rightarrow (NH_4)_2 GeF_6 + 2H_2O \qquad 2.12$$

From Equations 2.11 and 2.12, it is clear that the percentage of GeO_2 in the material influences the etching rate. By adjusting the ratio of NH_4F and *HF*, a tip or a cone can be fabricated on the fiber end [54]. When the ratio of NH_4F: *HF* is less than 1.7:1, the core has a faster etching rate than the cladding and this leads to an inverted cone on the fiber end; when the ratio of *NH4F*: *HF* is larger than 1.7:1, the cladding has a faster etching rate than the core and this leads to a tip on the fiber end as shown in Figure 2.5. To produce the air gap in the microgap structure, a cone ratio is applied.

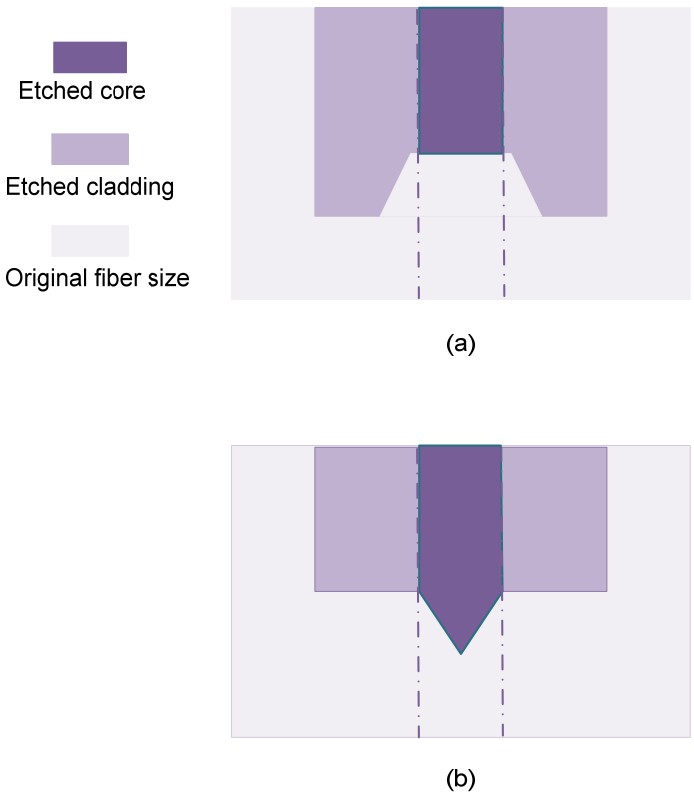

Figure 2.5 Illustration of selective etching of a GeO2 doped fiber in (a) a cone shape (*NH4F*: *HF* ≤ 1.7:1) (b) a tip shape (*NH4F*: *HF* ≥ 1.7:1)

In fiber optics, splicing is another commonly used fabrication method and can be realized by arc fusion splicing machine with high accuracy. The arc fusion machine heats two straightly aligned fibers by a spark discharge resulting from a 2000-4000 voltage differential across the electrodes. Some parameters should be set to optimize the splicing. To achieve minimum splicing loss, several parameter combinations were tested. Table 2.1 summarizes the parameter values in this work.

Table 2.1 Splicing parameters for SMF and etched SMF

Parameters	Arc duration	Pre-fusion	Arc gap	Overlap	Arc power
Value	02.00	00.10	10.00	11.00	00.28

Once the parameters are set, splicing is automatically finished within the machine, and the whole process can be monitored from a screen. An estimated splicing loss is given by the machine and this is useful for judging the splicing quality.

Cleaving the other end of the etched fiber is the last step to make a sensor. The cutting position decides the length of the cavity. Based on the previous work [38, 55], the cavity length of a single-cavity Fabry-Perot should be less than approximately 100μm in order to achieve a better fringe visibility. Tilt angle and roughness of the end surface will reduce the reflection power. During the cleaving, the sensor is connected to a component test system (CTS) to monitor the spectrum quality and the cleaving is completed under a microscope.

The structure and fabrication of the microgap sensor described above can be further illustrated by Figure 2.6 and summarized below.

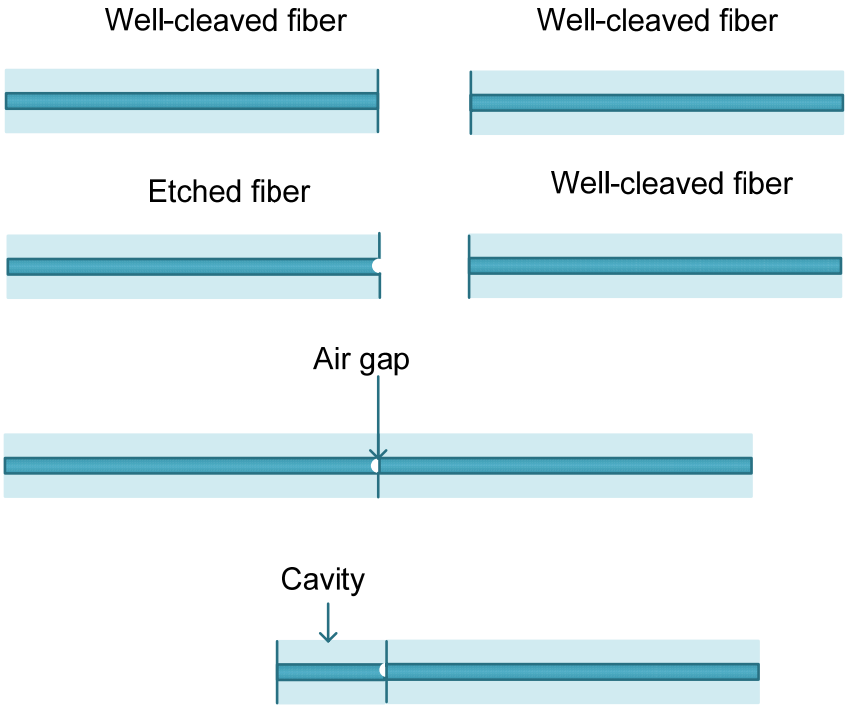

Figure 2.6 Illustration of microgap sensor fabrication

1. Cleave one single mode fiber under a microscope (Olympus SZ40 microscope) as the major fiber and measure its reflective spectrum with a component test system (Si720 Swept Laser Interrogator, Micro Optics) to generally judge the fiber end quality.

2. Cleave the second single mode fiber under the microscope.

3. Etch the second well-cleaved single mode fiber with a balanced solution of *HF* and NH_4F until a 1-2μm inverted cone is formed in the core area.

4. Manually splice the etched fiber to the lead fiber with pre-set parameters.

5. Cleave the other end of the etched fiber to form the FP cavity. This cleaving process is also monitored under the microscope. The sensor and the reflection spectrum are given in Figure 2.7.

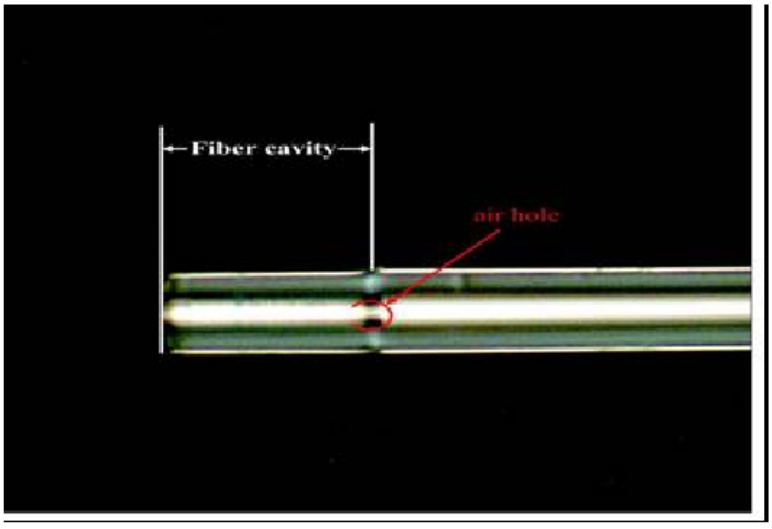

(a)

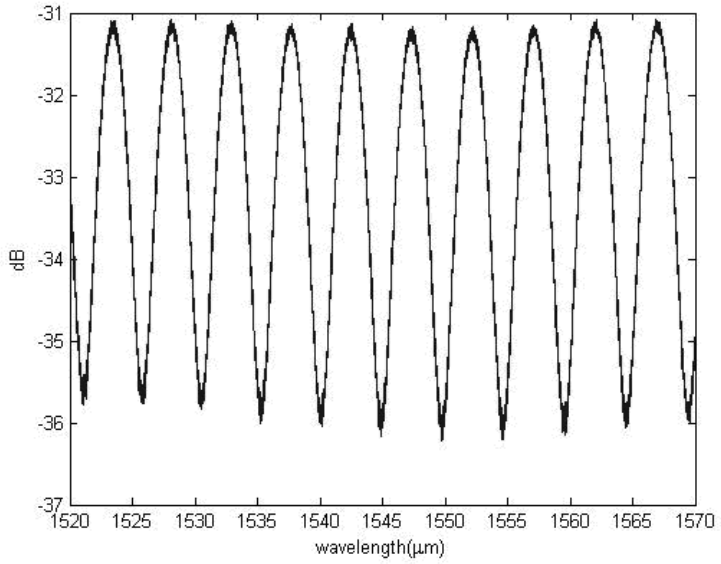

(b)

Figure 2.7 (a) Structure of microgap sensor (b) Spectrum of the microgap sensor obtained from component test system (Si720 Swept Laser Interrogator, Micron Optics)

After a sensor is fabricated, the far end will be modified by a layer-by-layer self-assembly technique. The probe DNA can be immobilized on the functionalized sensor tip. By measuring the cavity length change induced by specific binding between the probe DNA and the target DNA, label-free fast DNA detection can be achieved. The specific procedure will be introduced in the following chapters.

2.3 Measurement system

The measurement system consists of three major components as shown in Figure 2.8: a fiber holder, a component test system (Si720 Swept Laser Interrogator, Micro Optics), and a personal computer. The Si720 swept laser interrogator has an embedded laser source and the spectrum ranges from 1520nm to 1570nm. The laser can continuously sweep across the 50 nm spectrum at a rate of 5.0 or 0.5 Hz [56]. The sensor is connected to the component system through a 3dB coupler, and the sensor head is fixed on a fiber holder for

the convenience of successive operations. The data measured from the component test system is transferred to the computer via an Ethernet cable. Since the measurand is on the order of a nanometer, it requires the measurement system to be stable and clean. The entire experiment is completed in a stable, temperature-fixed environment.

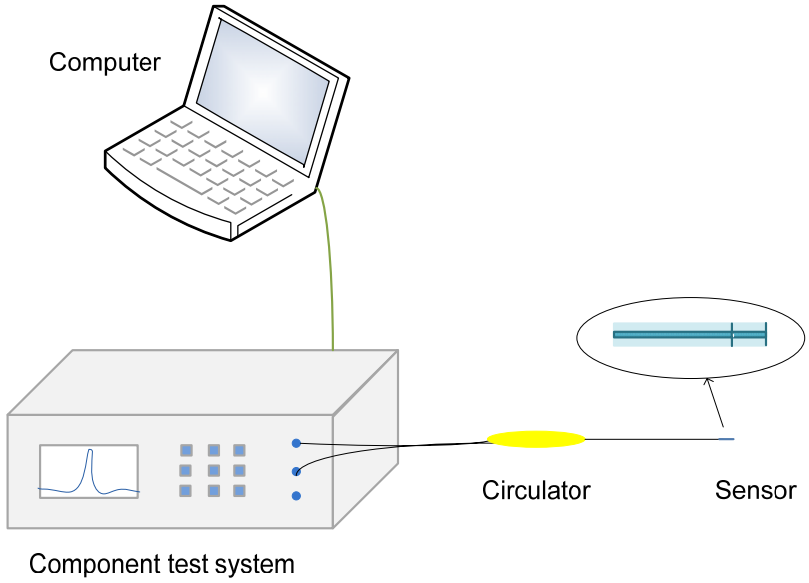

Figure 2.8 The sensor interrogation system

2.4 Signal processing

As discussed before, the Fabry-Perot interference spectrum is governed by Equation 2.1 as

$$I = I_1 + I_2 + 2\sqrt{I_1 I_2}\cos(\phi) \qquad 2.13$$

Here, ϕ is the total phase shift of the cavity, which can be expressed as:

$$\phi = 2\pi \frac{OPD}{\lambda} + \phi_0 \qquad 2.14$$

OPD is the optical path distance, defined by

$$OPD = 2nd \qquad 2.15$$

At the peaks of interference spectrum, we have

$$m = \frac{OPD}{\lambda} \qquad 2.16$$

where m is an integer number and differs by one between adjacent peaks. Therefore for two neighboring peaks λ_m and λ_{m+1}, we can derive:

$$OPD = m \times \lambda_m = (m+1) \times \lambda_{m=1} \qquad 2.17$$

From the spectrum, we can choose two adjacent peaks as λ_m and λ_{m+1} and calculate m from Equation 2.18. If we put m into Equation 2.17, the OPD can be calculated. This OPD has error of

$$\frac{\delta OPD}{OPD} = \frac{\delta\lambda}{\lambda} \qquad 2.18$$

where $\delta\lambda$ is the uncertainty of the peak wavelength measurement. By Equation 2.15, both the cavity physical length d and the refractive index n contribute to the OPD. Since this biosensor scheme is based on monitoring the cavity physical length variation, the refractive indices (RIs) of the fiber, the polymer and the DNA sample are assumed to be constant. Usually the RI of the core of a single mode optical fiber is approximately1.46, and the RI of the polymer can be tuned by controlling the pH and solution concentrations during the film growth [28].

Chapter 3 Surface modification by layer-by-layer electrostatic self-assembly method

3.1 Layer-by-layer electrostatic self-assembly method

As described in the proceeding chapters, a reliable receptor, which can stably combine a specific analyte with a transducer, is pursued in biosensing. For optical biosensors, some SiO_2 based immobilization techniques have been investigated such as the covalent bonding method [57-59], the Langmuir-Blodgett (LB) technique [60], and the electrostatic self-assembly technique (ESA) [61]. Covalent bonding method is based on the activation of the underlying planar surface and the modification of the DNA molecule with metal charges. It is usually limited by the complex preparation process. In comparison, thin organic films employed by the LB technology and the electrostatic self-assembly technique are more efficient and economic. The LB technique builds multilayer nanostructure thin films by water mechanical force. The outer layer can be hydrophobic or hydrophilic depending on the last deposition. This commonly-used method is limited by the molecular choosing in some applications. ESA forms multilayer thin films based on electrostatic force between the oppositely-charged polymers. It has been employed to embed molecules into an optical transducer as a feasible receptor [62].

Iler presented the idea of constructing multilayer films composed of positively and negatively charged colloidal particles in 1966 [63]. In1990, Decher and Kunitake followed this idea and further introduced the fabrication of multilayer polymeric thin films with oppositely-charged polyelectrolyte, which is the basic theme of layer-by-layer electrostatic self-assembly method (ESA). In recent years, ESA has been widely

investigated as a popular nanofabrication technology [64, 65]. The fabrication process can be described as alternately depositing oppositely charged monolayers on the substrate surface, as shown in Figure 3.1. The electrical attraction force between polycations (positively charged organic polyelectrolyte) and polyanions (negatively charged organic polyelectrolyte) builds uniform and stable multi-films. One pair of polycation layer and polyanion layer is referred as one bilayer and the film thickness is linear with the number of bilayers. This film structure provides the freedom of controlling the thickness at the molecular level, usually on the order of angstroms. In addition, the film details can be tuned by some other parameters such as pH value, salt concentration, polymer species and substrate conditions [66]. The environment conditions such as temperature and humility can influence the stability of thin films. ESA provides the flexibility of structure details and can be realized in room temperature, so it is attractive and low cost.

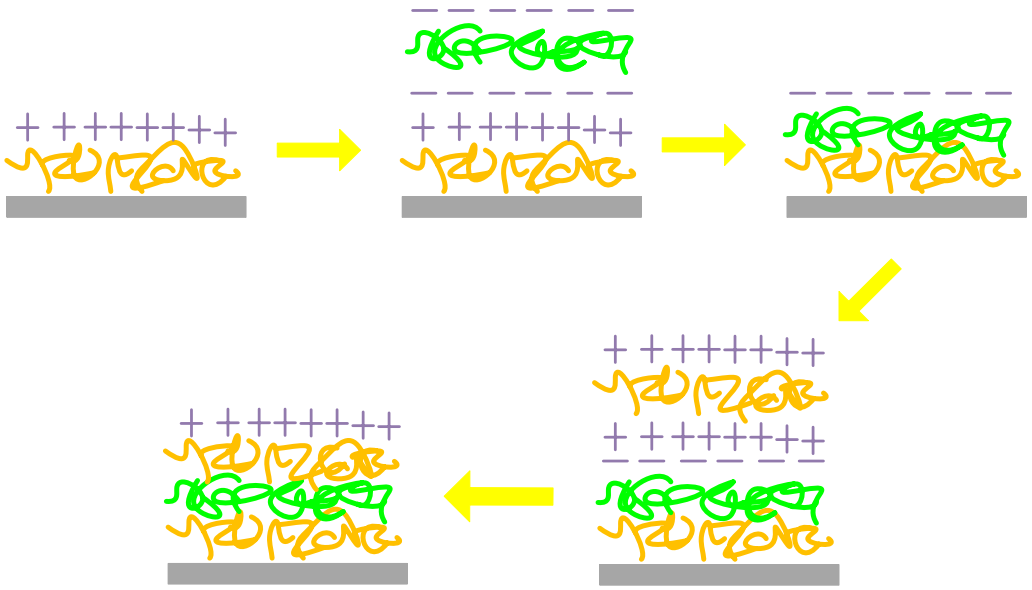

Figure 3.1 Scheme diagram of layer-by-layer electrostatic self-assembly method

One advantage of ESA is that the chemical properties of the polymers are preserved after the multilayer buildup. Thus some interesting material can be bonded on the films by chemical interactions such as hydrogen bonds [67], covalent bonds [68], and specific recognition [69]. Much work has been generalized to incorporate molecules, proteins and

macromolecules into polymers [62, 64, 70-73]. In this thesis, a probe DNA strand was immobilized onto the polymer surface; meanwhile the probe DNA kept the activity to hybridize with a target DNA strand. This characteristic of ESA paves the way for the further sensing function.

ESA is also attractive in surface modification applications. For optical biosensors, it is difficult to directly immobilize a specific molecule with activity onto the silica surface. For example, proteins will be denatured if they are bonded on silica surface by the forces flattening the molecules against the surface [74]. In this sense, ESA can functionalize the silica surface as a precursor, and specific molecules can be subsequently immobilized on the polymers with high activity. Experiment has demonstrated that ESA is an effective tool to realize surface modification and lays the foundation for biosensor investigations [62].

3.2 Factors controlling the polymer growth

Although the principle of ESA can be simply interpreted as alternately dipping the substrate into oppositely-charged polymer solutions, the nature of the film growth process is more complicated and governed by an array of factors such as pH value, salt concentration, polymer species and substrate material. Researchers have taken a great effort to deeply understand the fundamental relationship and control the process in details. Several methods that are often used to characterize ESA films include ellipsometry [75], X-ray reflectometry [64], near-field scanning optical microscopy [76] and atomic force microscopy [77]. It has been demonstrated that polyelectrolytes can bond with the underlying substrate adhesively due to ionic bonds. Since the charge density of the substrate is different with that of the polymers, the first layer deposition between the substrate and the polymer varies slightly with the successive depositions between polymers.

The adsorption of the incoming polymer layer is more related with the charge density of the underlying layer [78]. Accordingly, the first layer deposition can minimize the influence of the underlying substrate and the successive depositions show a linear relationship with the number of layers after the first depositon. This feature is the foundation to build uniform and thickness-adjustable thin films on the order of nanometer. In addition, it has been disclosed that the conformation and thickness of monolayer depend on the pH value of the polymer solutions [79], because the pH value can change the charge density of solutions. It has been reported that the thickness of the same monolayer can change from 0.5 nm to 8nm under different pH conditions. A variety of groups are working on the explanation of those phenomena and many models have been given [79-81]. Besides, the thickness of polyelectrolyte multilayer is sensitive to salt concentration. This can be addressed from the adsorption between the oppositely-charged polyelectrolytes. The adsorption is considered as an ion exchange process, during which the charged polymer segments replace small ions and compensate the surface charge. In this sense, salt concentration changes the number of small ions, and further influences how the charged polymer segments compensate the surface charge [82]. At the same time, other factors such as polymer concentration, rising procedure, and immersion time also affect the polyelectrolyte deposition quality.

In this work, ESA serves as a precursor to immobilize a probe DNA onto the sensor head, so the stability and the repeatability of ESA affect the immobilization of the probe DNA. The film deposition on the fiber tip can increase the optical length of the Fabry-Perot cavity. The total deposition effect of several factors to the optical length (the product of the physical length and refractive index) is more meaningful for experiment design. To investigate the total effect, a series of experiments with different parameters were conducted [83]. Five major factors were examined in previous experiments: pH value,

polymer species, polymer concentration, salt concentration and dipping time. With MINITAB (Minitab Inc), 8 combinations of 5 factors were compared based on the analysis of the physical length and the analysis of refractive index separately. In conclusion, the variation of the physical thickness due to the five factors play a dominant role in the optical length compared with that of refractive index [83]. Thus the factors, which change the physical thickness significantly, are first considered. Polymer species and salt concentration are two major factors to change the physical thickness. Other factors such as PH, polymer concentration and dipping time can be tuned according to the requirement. All parameters in the following experiment were selected based on the optimal consideration.

3.3 Assembly of thin films on the fiber end

Before immobilizing a single-strand DNA onto the fiber end using ESA, it is necessary to understand the characteristics of the self-assembled films on the fiber. The optical length incensement due to the thin films can be calculated from the reflection spectrum of the microgap sensor. The setup to exam the film characteristics is illustrated in Figure 3.2. Here the assembling of polyelectrolyte films onto the fiber will be formatted as the increase of optical path distance (*OPD*).

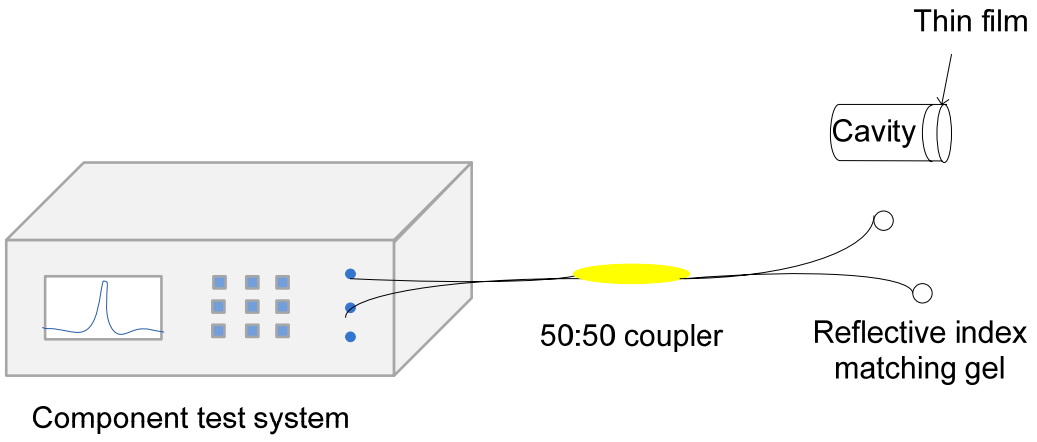

Figure 3.2 Experimental setup of thin film measurement

3.3.1 Material preparation

ESA can be simply described as alternatively depositing the polycations and polyanions films on the fiber end. Polyallylamine hydrochloride (*PAH*, Aldrich Inc) was selected as polycations and Polysodium 4-styrenesulfonate (*PSS*, Aldrich Inc) was selected as polyanions. Sodium Chloride (*NaCl*, Mallinckrodt Inc) was used to adjust the salt concentration. All the solutions were prepared with ultrapure deionized water (*DI* water, Barnstead Diamond system, 18MΩ). Hydrochloric acid (*HCl*) and sodium hydroxide (*NaOH*) were used to adjust the PH value of the solution and Corning 455 Ion Analyzer was used to test the PH value. The material preparation steps are summarized as below:

1. Make *NaCl* solution with ultrapure *DI* water and *NaCl* powder. Calculate and weight the required salt using a clean sheet of weigh paper. Sonicate the salt with the required volume of *DI* water in an Erlenmeyer flask.

2. Polymer solution preparation. Calculate and weight certain volume polymer powder or solution. Measure the prepared salt water based on calculation. Put the polymer sample and the measured water in a beaker. Seal the beaker with a thin film and stir the solution overnight.

3. Adjust the PH value of the solution to 7. First test the solution with a PH paper, if the PH value is higher than 7, add 0.1mol/ml *HCl* drop by drop with a syringe, and test the PH value again. If the PH value is less than 7, add 0.1mol/ml *NaOH* drop by drop with the syringe. Repeat the procedure until the PH value falls in the required range.

Table 3.1 Parameters of Polymer solution

Polymer	Volume	Concentration	Salt concentration	PH
PAH	30ml	4mg/ml	0.15M	7
PSS	30ml	4mg/ml	0.15M	7

3.3.2 Assembling procedure

Before coating the polymer, the fiber end was rinsed in piranha solution (H_2SO_4: H_2O_2= 7: 3 v/v) at room temperature in a fume hood. A thin silica layer (2 nm) was naturally grown on the silicon surface due to oxidization, which generated negative charge in water or solutions primarily due to the dissociation of terminal silanol groups [28]. After rinsing process, the fiber end was considered as negative-charged, thus ESA began with the positive polymer. The process can be described by the following steps:

Step 1: Insert the sensor in piranha solution (H_2SO_4: H_2O_2= 7: 3 v/v) for 10 minutes and wash it with *DI* water. The sensor tip is negatively-charged.

Step 2: Dry the sensor and test the cavity length in the air and record the spectrum.

Step 3: Immerse the fiber sensor into *PAH* solution for 6 minutes, and the sensor head is positively charged. Rinse the fiber sensor with *DI* water in ultrasonic meter three times.

Step 4: Dry the sensor and test the cavity length in the air.

Step 5: Immerse the sensor into *PSS* solution for 6 minutes, and the sensor head is negatively charged. Rinse the sensor with *DI* water three times.

Step 6: Dry the sensor and test the cavity length in the air.

Step 7: Repeat step3-step 7 for 10 bilayers. The immersing time for each layer can be reduced to 3 minutes. Keep the out layer positively-charged.

Step 8: Dry the sensor with a stream of nitrogen (N_2).

3.3.3 Result and analysis

$[PAH/PSS]_{10}$ polymers were assembled on the surface of the microgap FP sensor. The optical length of each layer can be calculated from the spectrum. As shown in Figure 3.3, the optical length of the sensor increased linearly with the number of polymer layers.

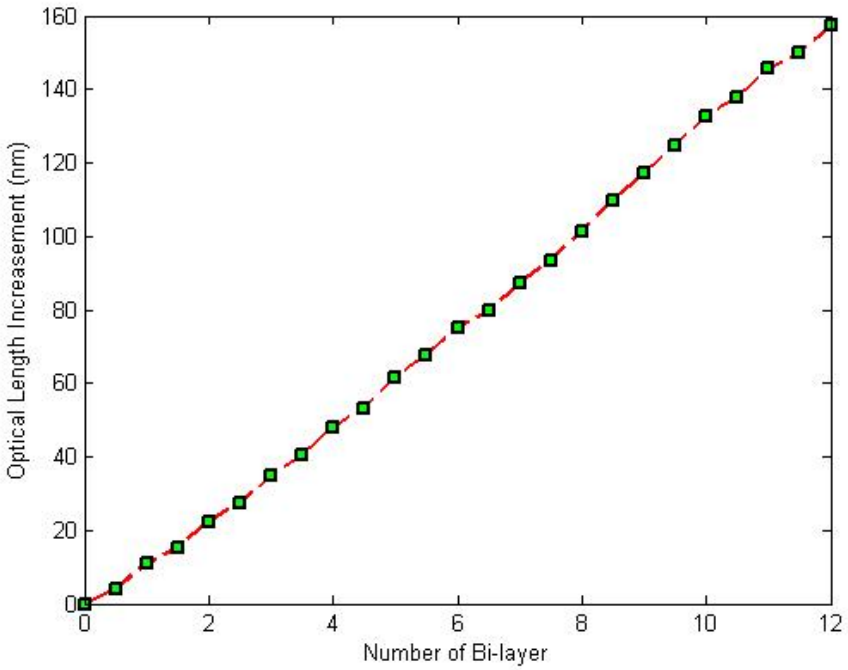

Figure 3.3 Optical length increase of $[PAH/PSS]_{12}$

The optical length is the product of refractive index and the physical length. The refractive index of [*PAH/PSS*] is 1.54 from the ellipsometry measurement and the physical

length of each *PAH/PSS* bilayer is 8.3nm (STD=0.6nm). *PAH* and *PSS* contribute to each bilayer differently in length. From Figure 3.4, *PAH* with a physical length of 3.4nm (STD=0.45nm) is thinner than *PSS*, which is 4.9nm (STD=0.3nm). This experiment result is consistent with previous experiment results [7, 83].

The repeatability and the stability of the self-assembled polymers were examined. Assembling process was repeated with [*PAH/PSS*] polymers. Comparing the results of two trials, the increase trends of the optical length are the same as shown in Figure 3.5. The stability of films was investigated by measuring the optical length of films in 2 weeks after the deposition and the optical length varied within ± 0.1 nm per layer. This phenomenon can be explained by the release of water molecules from the film and reentry from the air due to environment temperature and humidity [83].

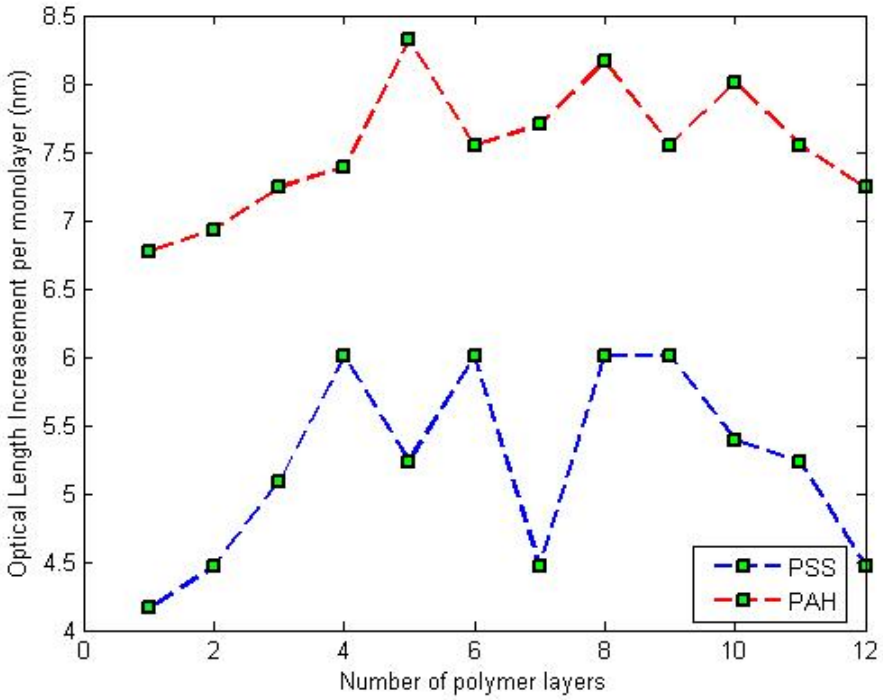

Figure 3.4 The monolayer thickness of PAH and PSS

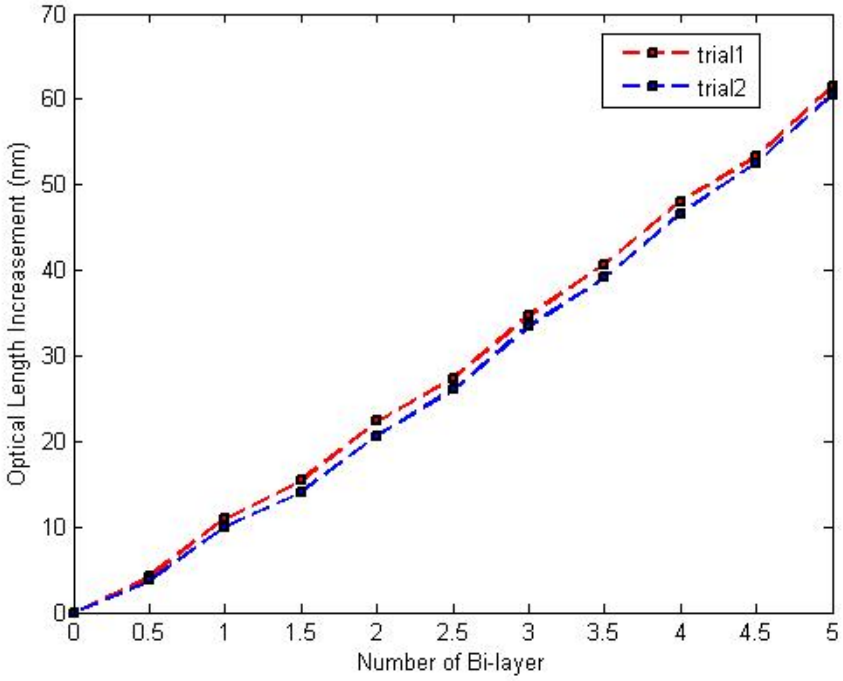

Figure 3.5 Experiment results of two thin films deposition trials

3.4 Conclusion

In this chapter, the concept and procedure of the electrostatic self-assembly method were introduced. The factors that influence ESA film qualities were given. It has been successfully demonstrated that building the thin films onto the fiber end with ESA is feasible. The thickness of the thin films was measured by a microgap sensor with high sensitivity. The stability and the repeatability of the thin film make it suitable as a biosensing precursor.

The microgap sensor has high sensitivity for the thin film measurement. Single layer deposition can be monitored accurately. ESA provides a way to modify the fiber end without damaging the biological activity. Combined with ESA, the microgap sensor is an effective tool to investigate the thin films, and further to investigate some molecules.

Chapter 4 Probe DNA Immobilization and Label-free Target DNA Detection

4.1 Introduction

Deoxyribonucleic acid (DNA) is a long polymer, which contains the genetic information in living organisms and some viruses. The main function of DNA is to store and translate the information. It plays an important role in rebuilding cells from generation to generation.

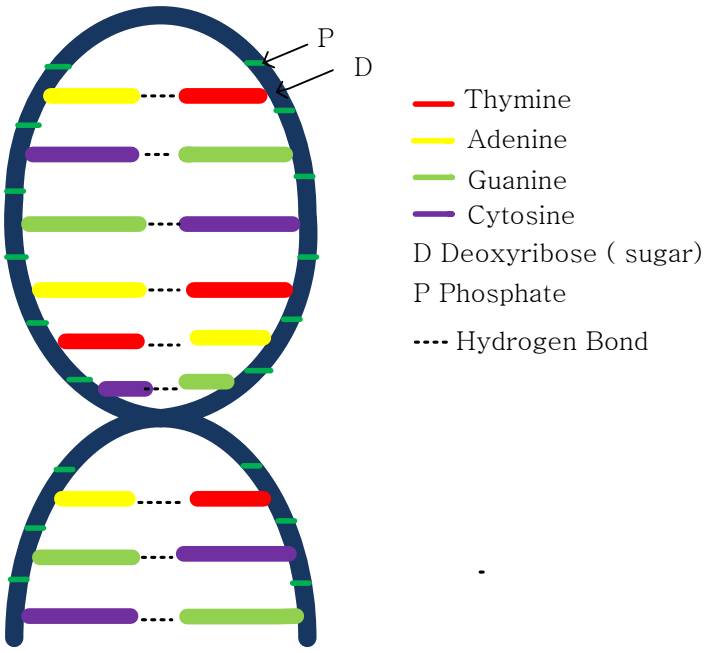

Figure 4.1 Double-helix structure of DNA molecule

A DNA molecule has a double-helix structure as shown in Figure 4.1. The sides of the ladders are composed of alternating sugars (deoxyribose and phosphates); the rungs of the ladder are composed of nucleotides. Nucleotides are basic building units of DNA

molecule and different in nitrogen bases. There are four kinds of nitrogen bases: Adenine (A), Thymine (T), Guanine (G) and Cytosine (C). Two specific pairs are exclusively formed between bases: A and T link with two hydrogen bonds (non-covalent); G and C link with three hydrogen bonds [84]. Each side of the ladder is defined as a single strand and two long strands entwine like vines, in the shape of a double helix. It is a specific sequence of bases that transmits the genetic codes. Hybridization between two strands is a selective recognizing process, thus one strand can be attached on the sensor tip as a probe strand to detect a complementary target strand in the solution.

With the progress of human genetic project, it is required to fabricate an efficient sensor to analyze DNA information for the diagnosis application and genetic understanding. In this research, an optical fiber based sensor was designed to realize a fast label-free DNA sequence identification. This sensor shares the same principle with classic biosensors: a biological receptor senses the variation of measurand and a transducer interprets the variation into measurable signals. A single strand DNA (probe DNA) with a known base sequence was used as a biological receptor. A microgap Fabry-Perot interferometer was used as a transducer, interrogating the optical cavity length variation. Considering the sugar phosphate backbone, DNA can be regarded as a kind of negative polymer, thus layer-by-layer electrostatic self-assembly technique was applied to immobilize a single strand DNA (probe DNA strand) to the surface-modified sensor. Since the hybridization between two strand DNAs are exclusive process, only the complementary DNA (target DNA strand) can hybridize with the probe DNA. If hybridization occurs, the optical cavity length of the sensor will increase as shown in Figure 4.2. By demodulating the interference pattern, the cavity difference can be calculated and finally the probe DNA detection can be achieved.

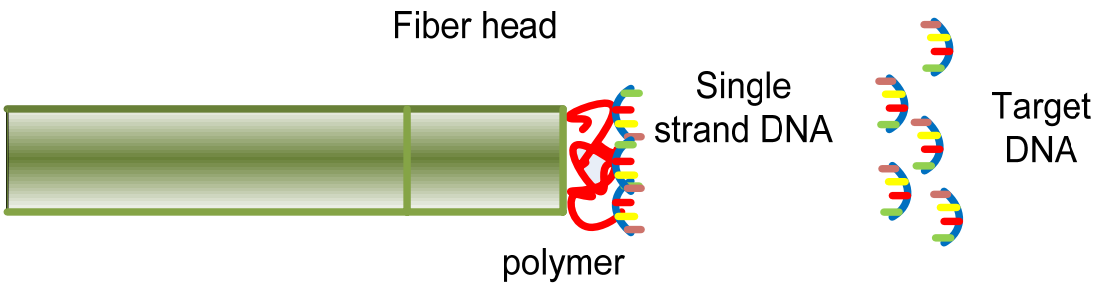

Figure 4.2 DNA detection scheme of mirogap sensor

4.2 Immobilization of single strand DNA

It is essential to maintain the activity of a biological receptor when attaching it to the sensor end. The silica material of optical fiber can adsorb proteins [74], but proteins are denatured due to the hydrogen-bonded configuration break in this adsorption. Thus modification of the optical fiber surface is necessary before the immobilization of probe DNA. A popular method of attaching DNA molecule to planar surfaces is covalent coupling. In this method, there is a demand to modify the DNA molecule with amino, thiol or biotin groups [57-59], which increases the complexity and the cost of process. In contrast, ESA is a fast and convenient way to modify the fiber surface as introduced early. With ESA method, the thin film thickness is adjustable on the nanometer scale and the outside layer polarity is controllable since positive and negative charged layer are built alternately. Also the feasibility and the stability of polymers on fiber end have been investigated. Due to the sugar phosphate backbone, single strand DNA can be considered as negative charged. Thus ESA method is an effective solution to immobilize single strand DNA onto the fiber end.

The backbone of a DNA strand is composed of phosphate and sugar residues [85]. The sugars connect each other with phosphodiester bonds between the third and fifth carbon atoms of adjacent sugar rings. These bonds are asymmetric, resulting that the direction of nucleotides in one strand is opposite to the direction in its complementary strand.

[28,85] Due to the asymmetric bonds, 5'end with a terminal phosphate group and 3' with a terminal hydroxyl group are used to different ends. In this experiment ssDNA is 26 mer in length as shown in Table 4.1.

Table 4.1 Probe DNA sequence

Name	Purpose	Sequence
ssDNA-A	Probe	5'-TCCAGACATGATAAGATACATTGATG-3'

The experimental setup of ssDNA immobilization is shown in Figure 4.3: a microgap sensor was connected with a component testing system (CTS, Micron Optics SI720) by a 3dB coupler. A computer processed the spectrum obtained from CTS and calculated the optical length variation due to the polymer deposition and ssDNA immobilization. *PAH* and *PSS* were selected as positive and negative polymers. *HCl* (a strong acid) and *NaOH* (a strong base) were used to adjust the pH value, which is monitored by Corning 455 Ion Analyzer. All water in the experiment was ultrapure deionized water. Solutions used in this experiment were prepared as shown in Table 4.2, and the process can be described as follow:

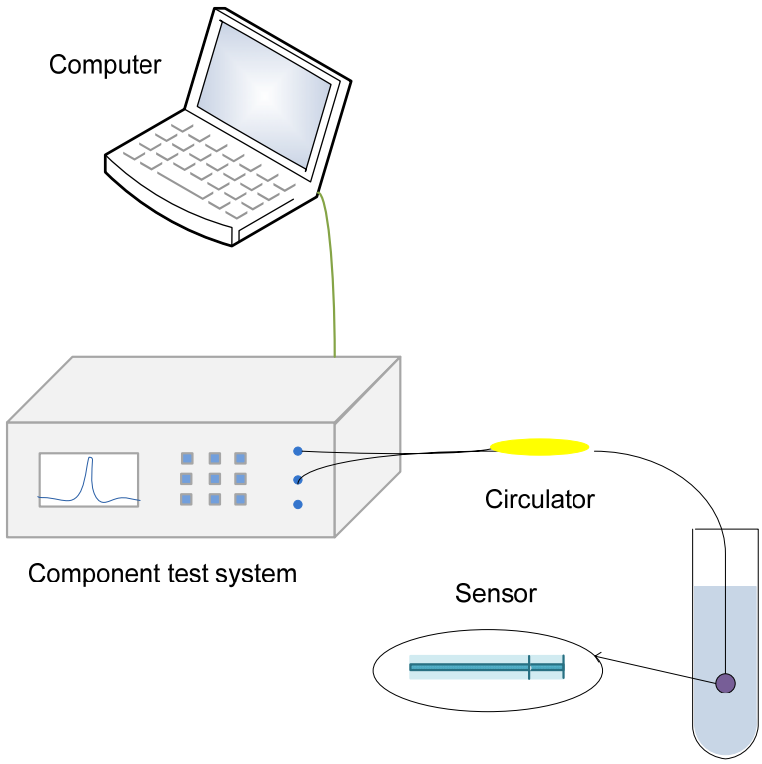

Figure 4.3 Setup of ssDNA immobilization experiment

Table 4.2 Parameters of solutions for DNA immobilization

Polymer	Volume	Concentration	Salt concentration	PH
PAH	30ml	4mg/ml	0.15M	7
PSS	30ml	4mg/ml	0.15M	7
ssDNA	30ml	65.7nmol/ml	0.02M	5

1. Rinse the sensor tip with piranha solution (H_2SO_4: H_2O_2 =7: 3 v/v)

2. Polymer thin film deposition on the sensor tip

- Begin with positively-charged polymer *PAH*

- Immerse the sensor tip into the polymer solutions 3 minutes for each layer. For the first polymer bilayers, use five-minute immersion time.

- Rinse the sensor thoroughly with *DI* water after each layer deposition

- Keep the outer layer positively-charged polymer *PAH*

3. Dry the sensor with nitrogen gas.

4. Measure the polymer thickness with the test system

5. Immobilize ssDNA onto the substrate.

   - Immersion the sensor tip into prepared ssDNA solution for 20 minutes

6. Dry the sensor with nitrogen gas.

7. Measure the DNA film thickness with the test system

8. Confirmation test: repeat 1-7 steps

The optical length was measured in air and in a stable aqueous environment separately after each immobilization. The refractive index of the immobilized DNA monolayer was assumed to be 1.462 [86], which is very close to the RI of optical fiber. Thus the RI of optical fiber was used to calculate the physical length change. Measurement results of the physical cavity length increase are shown in Figure 4.4. The unstretched or unperturbed conformation of the immobilized ssDNA can be considered as a Gaussion coil of Kuhn step model. If the immobilized ssDNA is aligned parallel to the fiber end surface, the increased cavity length will be the radius of gyration of a ssDNA chain (2nm); if the immobilized ssDNA is aligned perpendicular to the end surface, the increased cavity length will be the end-to-end distance of the chain, 5 nm [85]. Therefore the variation range of the increased length should be between these two extreme values, from 2nm to 5 nm. All the measurement results fell in this range, which indicated that the immobilizations were successful. The slight difference between each experiment may be caused by different random tilt angles [85, 87]. As a preliminary step to develop a sensor for *vitro* measurement, each immobilization was examined in a stable aqueous environment. The data shows that generally the physical length obtained in aqueous environment is slightly larger than that obtained in air. This may be related to the DNA chain topology. The ssDNA chains can extend from a rigid substrate to a molecular

brushlike structure if the salt concentration changes [85, 88]. Ultrapure water, which was used to simulate the stable aqueous environment, can reduce the salt concentration. The ability to be operated within an aqueous environment is essential for this biosensor considering *in-vitro* measurements.

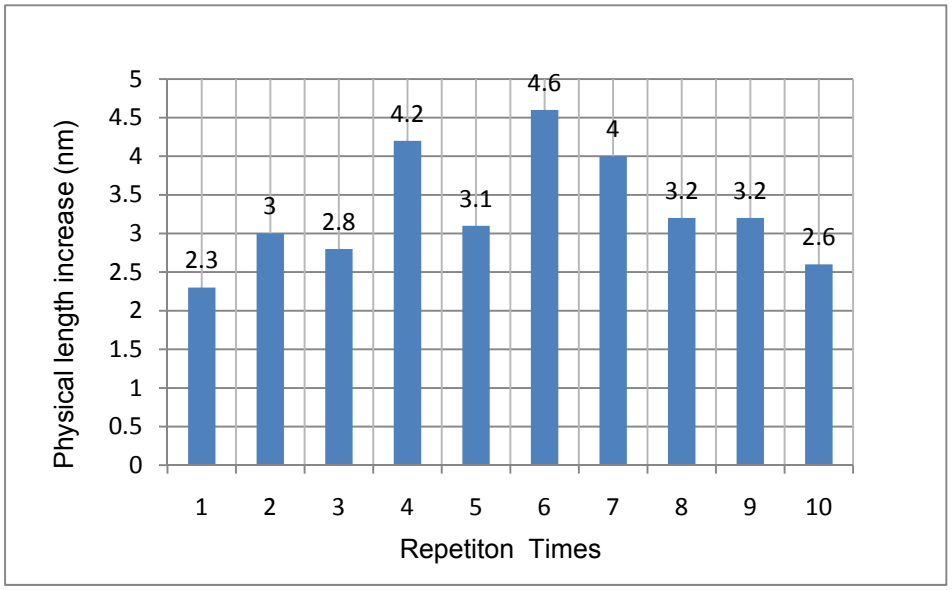

Figure 4.4 The physical length measurement in air after ssDNA immobilization

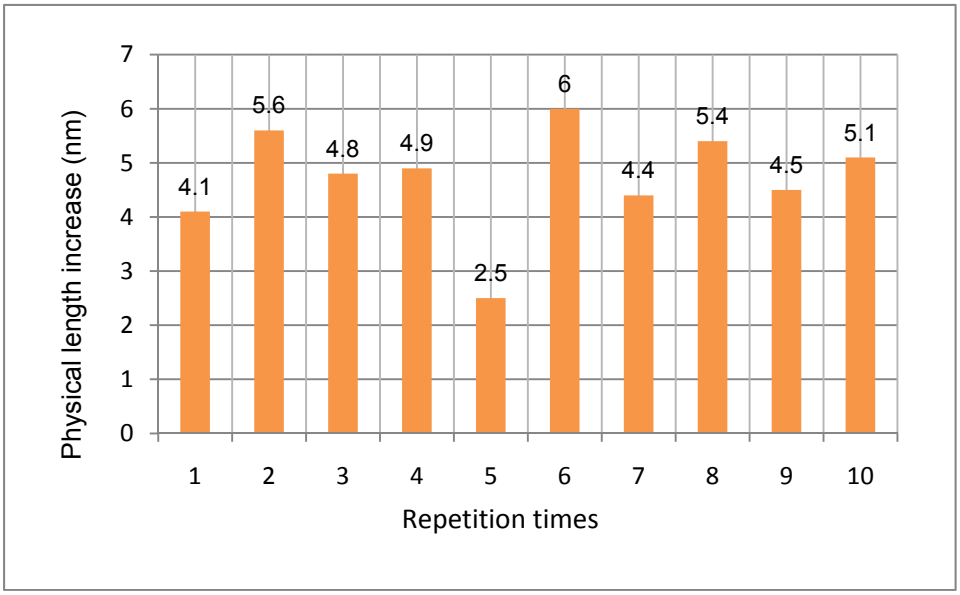

Figure 4.5 The physical length measurement in water after ssDNA immobilization

4.3 Hybridization of complementary DNA strand

Each type of base on one strand bonds with just one type of base on the other strand, as A bonding to T, and C bonding to G. This is called complementary base paring. Hydrogen bonds between two strands can be broken and rejoined due to the external conditions. At high temperature [89], hydrogen bonds turn to be thermodynamically unfavorable and complementary strands separate. Under normal conditions, complementary strands reanneal and form a "hybrid" molecule. This is a critical feature for DNA molecule to realize information translation from generation to generation. Hybridization is a process that two complementary single DNA strands combine into a single molecule. The specific interaction between complementary strands provides a feasible method to detect specific genes of DNA.

Table 4.3 DNA sequence for hybridization experiment

Name	Purpose	Sequence
ssDNA-A	Probe	5'-TCCAGACATGATAAGATACATTGATG-3'
ssDNA-B	Target	5'-CATCAATGTATCTTATCATGTCTGGA-3'
ssDNA-F	Negative control	5'-CTCACGTTAATTTTGGTC-3'

Table 4.4 Parameters of Polymer solutions and DNA solutions in hybridization experiment

Polymer	Volume	Concentration	Salt concentration	PH
PAH	30ml	4mg/ml	0.15M	7
PSS	30ml	4mg/ml	0.15M	7
ssDNA-A	30ml	65.7nmol/ml	0.02M	5
ssDNA-B	30ml	52.5nmol/ml	0.02M	5
ssDNA-F	30ml	128.3nmol/ml	0.02M	5

Based on the exclusive combination between complementary DNA strands, label-free DNA detection scheme was presented. First, the surface of a microgap sensor was modified with layer-by-layer electrostatic self-assembly method. Secondly a single strand DNA of known sequence was attached to the sensor head as a probe. Finally, hybridization would happen if the probe was dipped into a complementary strand DNA solution. The successful hybridization resulted in the increase of cavity length. This experiment shared the same setup and signal modulation theory with the DNA immobilization experiment. To keep consistency with previous DNA detection work [28], three kinds of DNA with different sequences, which served as probe DNA, complementary DNA and negative control sample respectively, are listed in Table 4.3. Solutions used in this experiment were prepared as shown in Table 4.4, and process can be described as follow:

1. Rinse the sensor tip with piranha solution (H_2SO_4: H_2O_2 =7: 3 v/v)
2. Polymer thin films deposition on the sensor tip
   - Begin with positive-charged polymer *PAH*
- Immerse the sensor tip into polymer solutions 3 minutes for each layer. For the first polymer bilayers, use five-minute immersion time
   - Rinse the sensor thoroughly with ultra pure water after each layer deposition
   - Keep the out layer positive-charged polymer *PAH*
3. Dry the sensor with nitrogen gas.
4. Measure the polymer thickness with the test system
5. Immobilize DNA onto the substrate.
   - Immersion the sensor tip into the prepared ssDNA-A solution for 20 minutes
6. Dry the sensor with nitrogen gas.
7. Measure the DNA film thickness with the test system

8. Hybridization test

- Immersion the sensor tip into the prepared ssDNA-B solution for 20 minutes

9. Dry with nitrogen gas.

10. Measure the DNA film thickness with the test system

11. Compare experiment

-Repeat 1-7 steps

- Immersion the sensor tip into prepared ssDNA-F solution for 40 minutes

-Dry the sensor with nitrogen gas.

- Measure the DNA film thickness with the test system

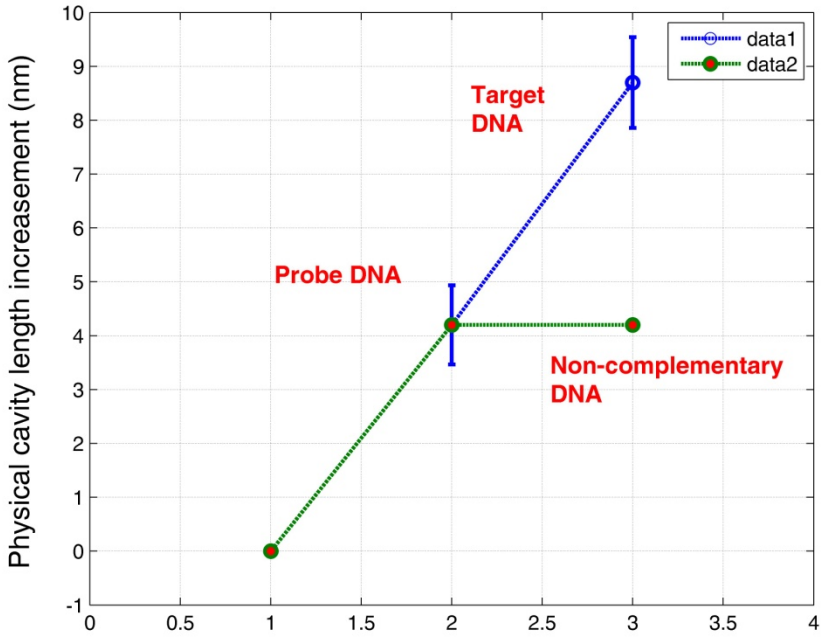

Figure 4.6 Hybridization of complementary DNA on sensor tip

If hybridization occurs, duplexes will form; this newly-formed double-strand DNA (dsDNA) will result in a cavity length increase. Otherwise, unhybridized ssDNA-B will be rinsed away and no cavity length increase will be observed. As shown in Figure 4.6, the cavity length was increased by 4.5nm physically (Optical length divided by refractive

index n=1.45) due to the complementary DNA. Depending on the configuration of dsDNA, the increase length can vary from 2nm-5nm [85]. This result is consistent with reference [28] and indicates that microgap sensor can detect complementary DNA sequence successfully. To test the sensor performance with non-complementary DNA sequence, negative control test is conducted. From the results shown in Figure 4.5, although the concentration of non-complementary ssDNA-F was higher and reaction time was longer, the length of cavity did not change. This indicates that this sensor is capable of detecting a specific sequence DNA.

4.4 Sensitivity and specificity of the biosensor

Since this work aims to produce a diagnostics biosensor, it is meaningful to investigate the sensitivity and specificity of this sensor. Sensitivity in this experiment describes the capability of DNA sensor to response to a target DNA. Specificity describes the ability of DNA sensor to recognize a particular sequence DNA.

4.4.1 Sensitivity of the biosensor

In this experiment, ssDNA-A and ssDNA-B served as probe DNA and target DNA respectively. To determine the sensitivity of the sensor, the concentration of the complementary ssDNA-B was reduced by half after successful hybridizations until no hybridization was detected. Polymer solutions used in this experiment were prepared as the same parameters as previous experiments. Since the measurand is on the order of a micron, a little environment disturbance such as person walking, airflow from air-condition, may lead to instable signal. So the experiment is separately conducted in the chemistry room under a constant temperature. The procedure is described as follow：

1. DNA sensor is functionalized with 5.5 bilayer [*PAH/PSS*] polymer. Measure the cavity length as baseline.

2. Immobilize the ssDNA-A (65.7nmol/ml) onto the probe tip, measure the cavity length and compare it with baseline to judge whether the immobilization is successful

3. If the immobilization of ssDNA is successful, begin the hybridization test with 70.5nmol/ml ssDNA-B. Measure the cavity length and judge whether the hybridization happens or not.

4. If the hybridization is successful, reduce the concentration of ssDNA-B solution by half and repeat 1-4 steps with the same sensor until no hybridization happen.

5. Confirmation experiment: repeat hybridization test with the lowest concentration ssDNA-B solution.

As shown in Figure 4.7, the cavity length increased after each successful hybridization test. The increase length varied from 2.0nm to 4.5nm for different test rounds; this may be related to the DNA chain topology. Also the salt concentration can cause the difference in thickness. At low *NaCl* concentrations, the negative charges on the DNA chain tend to repel each other, stretching the DNA strands. When the concentration of *NaCl* increases, the Na^+ alleviate the repulsion, and the DNA strands may coil up [28]. The results show that the detection limit of this structure sensor was found to be 6nmol/ml.

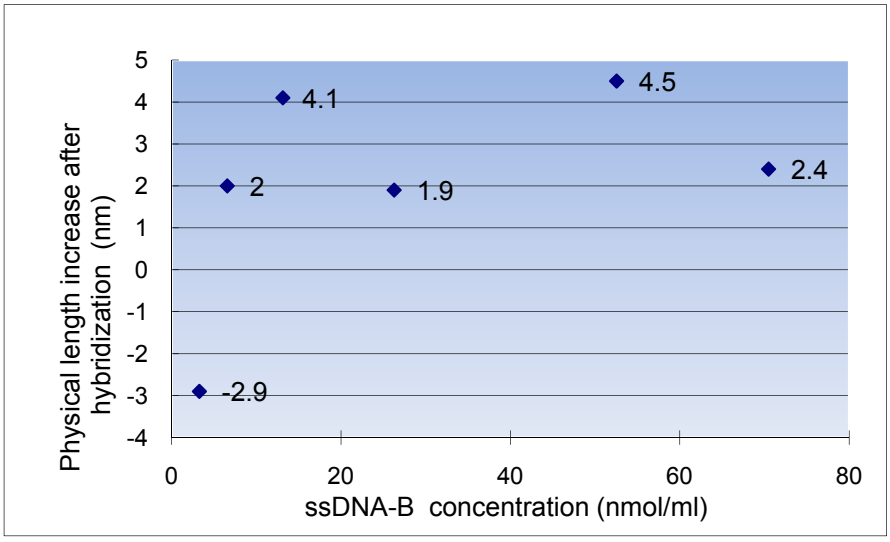

Figure 4.7 Hybridization sensitivity test

4.4.2 Specificity of the biosensor

The DNA sequence records the genetic information with different sequences of four basic bases: A, T, G, C. The number of bases in each strand describes the length of DNA. A great diversity of DNA sequences can be different from length; also can be different from base sequence even with the same length. Some DNA strands resemble each other only with a few different base bits. Thus it is highly desired to recognize one DNA sequence accurately. To investigate the specificity of this DNA senor, a group of comparison experiments were conducted. The general idea is to do hybridization test by decreasing the number of base pair (bp) mismatches in the ssDNA solution. As given in Table 4.5, all DNA sequences in this experiment had the same length except the negative-control one, which has different length and completely unmatched bases. All DNA sample were prepared as shown in Table 4.6. The experiment steps are described as follow：

Table 4.5 DNA sequence in specificity test

Name	Purpose	Sequence
ssDNA-A	Probe	5'-TCCAGACATGATAAGATACATTGATG-3'
ssDNA-B	Target	5'-CATCAATGTATCTTATCATGTCTGGA-3'
ssDNA-C	2 bp mismatch	5'-CTTCAATCTATCTTATCATGTCTGGA-3'
ssDNA-D	5 bp mismatch	5'-CTTCAATCTATCTTTTCATGTCTCCA-3'
ssDNA-E	10 bp mismatch	5'-CTAGTATGAATGTAATGATGTCTCCA-3'
ssDNA-F	Negative control	5'-CTCACGTTAATTTTGGTC-3'

Table 4.6 Parameters of Polymer solution and DNA solution in hybridization experiment

Polymer	Volume	Concentration	Salt concentration	PH
PAH	30ml	4mg/ml	0.15M	7
PSS	30ml	4mg/ml	0.15M	7
ssDNA-A	30ml	65.7nmol/ml	0.02M	5
ssDNA-B	30ml	52.5nmol/ml	0.02M	5
ssDNA-C	30ml	138nmol/ml	0.02M	5
ssDNA-D	30ml	151.6nmol/ml	0.02M	5
ssDNA-E	30ml	145.4nmol/ml	0.02M	5
ssDNA-F	30ml	128.3nmol/ml	0.02M	5

1. DNA sensor is functionalized with 5.5 bilayer [*PAH/PSS*] polymer. Measure the cavity length as baseline.

2. Immobilize the ssDNA-A (65.7nmol/ml) onto the probe tip, measure the cavity length and compare it with baseline to judge whether the immobilization is successful.

3. If the immobilization of ssDNA is successful, begin the hybridization test with negative control ssDNA-F. Measure the cavity length and judge whether the hybridization happens or not.

4. If the hybridization is not successful, repeat the hybridization test with 10-bp mismatch ssDNA-C, 5bp-mismatch ssDNA-D, 2bp-mismatch ssDNA-C, Target ssDNA-B with the same sensor until the hybridization is successful.

Figure 4.8 shows the experiment results of specificity test. A positive slope between probe immobilization and target detection indicates a positive result; negative or zero slope indicates a negative result. Although the idea of negative slope may raise questions in some fields, it is merely a result of a shift in the film water content. This DNA sensor has high specificity and can recognize 2bp mismatch DNA.

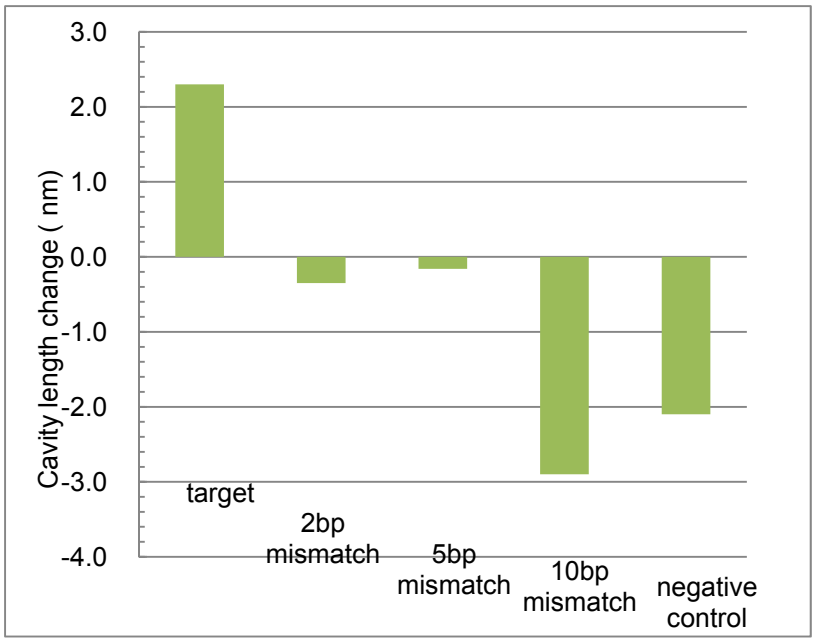

Figure 4.8 Hybridization specificity test

4.5 Summary

In this chapter, the ESA method was applied to immobilize a probe DNA onto the sensor tip. The results of immobilization and hybridization experiments demonstrated that the microgap sensor could be used as a biosensor. This sensor was investigated from the aspect of sensitivity and specificity and demonstrated with 2bp mismatch recognize ability.

In summary, the method is simple, low-cost, sequence specific, and sensitive to low concentration of the target DNA sequence. These advantages make it attractive in diagnosis applications. With the extra fiber etching or tapering process, the sensor size can be further reduced and may become even suitable for in-cell detection later.

Chapter 5 Conclusion and Future Work

5.1 Conclusion

Optical fiber sensors have developed fast and contributed to several sensing areas. The design of biomedical sensors based on optical fiber is a quite attractive area due to the intrinsic features of optical fibers, including small size, robustness, low cost and immunity to electromagnetic interference. In this work, one type of intrinsic fiber Fabry-Perot interferometric (IFPI) sensor was designed and fabricated for a fast label-free DNA detection.

Prior work demonstrated that the multicavity IFPI sensors could realize a label-free DNA sequence detection [88]. Based on this the prior result, this work presented a microgap IFPI, which possesses the advantages of easy fabrication, high signal-to-noise ratio and a simple demodulation algorithm compared with the multicavity sensor. The fabrication is simple and only involves fiber etching and splicing techniques. A microgap was formed by splicing one wet etched fiber to another fiber, serving as one mirror of the Fabry-Perot cavity. The encapsulated airgap between the two fibers functions as a reflection mirror and the other mirror was provided by a well-cleaved fiber end. The sensing is achieved by interrogating the cavity length, which can be modified by external conditions.

Electrostatic self-assembly (ESA) is an effective and convenient surface modification method and was applied in this work to bond the probe DNA to the fiber end. The thin film buildup process based on ESA was investigated with the microgap sensor. The

experiment results demonstrate that ESA can fulfill the objective. Detecting the hybridization event involves interrogating the optical cavity length variation resulted from the bonding between the target DNA strand and the probe DNA probe. If the hybridization is successful, the cavity length increases; otherwise the cavity length has no change or decrease. Sensitivity and specificity are widely used in statistics to describe a diagnostic test, so these characteristics were examined to evaluate this biosensor. Experiment results demonstrated that the detection limit of this sensor was 6nmol/ml and the mismatch recognizing ability is 2bp.

5.2 Future Work

Micro/nano fabrication can enable sensors to convey very small amounts of interesting information to the macroscopic world. Medical use of micro probes is mainly to identify particular cells in a human body. By measuring the changes in concentration, mass or pressure, the micro biosensor can distinguish some certain cells, such as cancer cells at the molecule level, thus they are very meaningful in diagnosis applications [90]. DNA sensors are highly concerned due to their important function of transferring genetic codes in living cells. Micro/nano fabrication of DNA sensor provides one way to fulfill the in-cell DNA detection. Once the DNA sensor is reduced down to cell scale, it would be possible to detect signs of the early DNA damage that can lead to cancers.

To realize the nanofabrication of DNA sensors, great efforts have been made by many organizations and different methods have been developed. Currently DNA nanotechnologies include DNA nanotube [91], fluorescence labeled optical fiber probe [92], and DNA layer incorporated COMS integral circuit [93]. As a biosensor, the optical fiber probe has the inherent features of small size and mechanical robustness. Meanwhile well-developed silicon based micron/nano fabrication technologies pave a

road for further reducing the size of the probe. It has been reported that a helium-cadmium laser beam excited nanofiber probe can penetrate a living cell [92]. However the pretreatment of coating fluorescent material on the probe in this scheme involves extra cumbersome work and the fluorescent signal detection usually requires a certain time. The DNA sensor presented in this thesis has been proved to be label-free and fast. Aiming at the in-cell DNA detection, the miniature sensor with the same structure is a new research direction of great interest.

Reference

1. Grattan, K. and B. Meggitt, *Optical fiber sensor technology: devices and technology*. 1998: Kluwer Academic Pub.
2. Chester, A., S. Martellucci, and A. Scheggi, *Optical fiber sensors*. 1967: Nijhoff.
3. Golnabi, H., *Mass measurement using an intensity-modulated optical fiber sensor.* Optics and Lasers in Engineering, 2002. **38**(6): p. 537-548.
4. Kurosawa, K. and K. Shirakawa, *Intensity modulation type optical sensor and optical current/voltage sensor*. 2006, Google Patents.
5. Thompson, R., *Fluorescence sensors and biosensors*. 2006: CRC.
6. Lo, Y. and T. Yu, *A polarimetric glucose sensor using a liquid-crystal polarization modulator driven by a sinusoidal signal.* Optics communications, 2006. **259**(1): p. 40-48.
7. Zhao, X., *Study of multimode extrinsic Fabry-Perot interferometric fiber optic sensor on biosensing*, in *ECE*. 2006, Virginia Polytechnic Institute and State University: Blacksburg,VA.
8. Jackson, D., *Recent progress in monomode fibre-optic sensors.* Measurement Science and Technology, 1994. **5**: p. 621.
9. Jacobson, K., *Biosensors and other medical and environmental probes.* ONRL Center for Biotechnology.[Online]. Available: http://www. ornl. gov/ORNLReview/rev29_3/text/biosens. htm.
10. Thévenot, D., et al., *Electrochemical biosensors: recommended definitions and classification* Analytical Letters, 2001. **34**(5): p. 635-659.
11. Pohanka, M. and P. Skladal, *Electrochemical biosensors–principles and applications.* J Appl Biomed, 2008. **6**(2): p. 57-64.
12. Deakin, M. and D. Buttry, *Electrochemical applications of the quartz crystal microbalance.* Anal. Chem, 1989. **61**(20): p. 1147A-1154A.
13. Storri, S., T. Santoni, and M. Mascini, *A piezoelectric biosensor for DNA hybridisation detection.* Analytical Letters, 1998. **31**(11): p. 1795-1808.
14. Babacan, S., et al., *Evaluation of antibody immobilization methods for piezoelectric biosensor application.* Biosensors and Bioelectronics, 2000. **15**(11-12): p. 615-621.
15. Wu, T., *A piezoelectric biosensor as an olfactory receptor for odour detection: electronic nose.* Biosensors and Bioelectronics, 1999. **14**(1): p. 9-18.
16. Ligler, F. and C. Taitt, *Optical biosensors: today and tomorrow*. 2008: Elsevier Science Ltd.
17. Raether, H., *Surface plasmons on smooth and rough surfaces and on gratings*. 1988: Springer-Verlag Berlin.
18. Wolfbeis, O., *Fibre optic sensors in biomedical sciences.* Fresenius' Journal of Analytical Chemistry, 1988. **330**(4): p. 336-336.
19. Schmitt, J., J. Meindl, and F. Mihm, *An integrated circuit-based optical sensor for in vivo measurement of blood oxygenation.* IEEE Transactions on Biomedical Engineering, 1986: p. 98-107.
20. Gehrich JL, L.D., Opitz N, Hansmann DR, Miller WW, Tusa JK, Yafuso M, *Optical Fluorescence and Its Application to an Intravascular Blood Gas Monitoring System*, in *IEEE Trans Biomed Eng*. 1986. p.

117-132.

21. Preininger, C., I. Klimant, and O. Wolfbeis, *Optical fiber sensor for biological oxygen demand.* Analytical Chemistry(Washington), 1994. **66**(11): p. 1841-1846.

22. Zhao, X., et al. *Characterization of DNA isolated from normal and cancerous ovarian tissues by ultraviolet resonance Raman spectroscopy*. 2000.

23. Vo-Dinh, T., *Nanobiosensors: probing the sanctuary of individual living cells.* Journal of Cellular Biochemistry, 2003. **87**(S39): p. 154-161.

24. Bartlett, J. and D. Stirling, *A short history of the polymerase chain reaction.* PCR protocols, 2003. **1501**: p. 3.

25. Lenigk, R., et al., *Surface characterization of a silicon-chip-based DNA microarray.* Langmuir, 2001. **17**(8): p. 2497-2501.

26. Betzig, E., et al., *Breaking the diffraction barrier: optical microscopy on a nanometric scale.* Science, 1991. **251**(5000): p. 1468.

27. Stöckle, R., et al., *High-quality near-field optical probes by tube etching.* Applied Physics Letters, 1999. **75**: p. 160.

28. Wang, X., *Label-free DNA sequence detection using oligonucleotide functionalized fiber probe with a miniature protrusion* in *ECE*. 2006, Virginia Polytechnic Institute and State University: Blacksburg, Va.

29. Qi, B., et al., *Novel data processing techniques for dispersive white light interferometer.* Optical Engineering, 2003. **42**: p. 3165.

30. Lee, C., et al., *Optical-fiber Fabry-Perot embedded sensor.* Optics letters, 1989. **14**(21): p. 1225-1227.

31. Betts, P. and J. Davis, *Bragg grating Fabry-Perot interferometer with variable finesse.* Optical Engineering, 2004. **43**: p. 1258.

32. Shen, F., et al. *UV-induced intrinsic Fabry-Perot interferometric fiber sensors*. 2004.

33. Kapron, F., D. Keck, and R. Maurer, *Radiation losses in glass optical waveguides.* Applied Physics Letters, 1970. **17**: p. 423.

34. Agrawal, G., *Fiber-optic communication systems*. 2004: Tsinghua University Pr.];: Wiley-Interscience.

35. Murata, H., *Handbook of optical fibers and cables*. 1996: CRC.

36. Bae, T., et al., *Interferometric fiber-optic sensor embedded in a spark plug for in-cylinder pressure measurement in engines.* Applied optics, 2003. **42**(6): p. 1003-1007.

37. Grossmann, B. and L. Huang, *Fiber optic sensor array for multi-dimensional strain measurement.* Smart Materials and Structures, 1998. **7**: p. 159-165.

38. Zhu, Y. and A. Wang, *Miniature fiber-optic pressure sensor.* IEEE Photonics Technology Letters, 2005. **17**(2): p. 447-449.

39. Qi, B., et al. *Fiber optic pressure and temperature sensors for oil down hole application*. 2002.

40. Bhatia, V., et al., *Multiple strain state measurements using conventional and absolute optical fiber-based extrinsic Fabry-Perot interferometric strain sensors.* Smart Materials and Structures, 1995. **4**: p. 240-245.

41. Sirkis, J., et al., *In-line fiber etalon (ILFE) fiber-optic strain sensors.* Lightwave Technology, Journal of, 1995. **13**(7): p. 1256-1263.

42. Chen, X., et al. *Novel Fabry-Perot fiber optic sensor with multiple applications*. 2004.

43. Peng, W., et al., *Self-compensating fiber optic flow sensor system and its field applications.* Applied optics, 2004. **43**(8): p. 1752-1760.

44. Wang, X., et al. *Verifying an all fused silica miniature optical fiber tip pressure sensor performance with turbine engine field test*. 2005.

45. Zhu, Y., et al., *High-temperature fiber-tip pressure sensor.* Lightwave Technology, Journal of, 2006. **24**(2): p. 861-869.

46. Lee, C. and H. Taylor, *Interferometric optical fibre sensors using internal mirrors.* Electronics Letters, 1988. **24**(4): p. 193-194.

47. Tsai, W. and C. Lin, *A novel structure for the intrinsic Fabry-Perot fiber-optic temperature sensor.* Journal of Lightwave Technology, 2001. **19**(5): p. 682.

48. Drummond, T., M. Hill, and J. Barton, *Electrochemical DNA sensors.* Nature biotechnology, 2003. **21**(10): p. 1192-1199.

49. Homola, J., *Present and future of surface plasmon resonance biosensors.* Analytical and bioanalytical chemistry, 2003. **377**(3): p. 528-539.

50. Piunno, P., et al., *Fiber optic biosensor for fluorimetric detection of DNA hybridization.* Analytica Chimica Acta, 1994. **288**(3): p. 205-214.

51. Hoffmann, P., B. Dutoit, and R. Salathe, *Comparison of mechanically drawn and protection layer chemically etched optical fiber tips.* Ultramicroscopy, 1995. **61**(1-4): p. 165-170.

52. Epstein, J., M. Lee, and D. Walt, *High-density fiber-optic genosensor microsphere array capable of zeptomole detection limits.* Anal. Chem, 2002. **74**(8): p. 1836-1840.

53. Puygranier, B. and P. Dawson, *Chemical etching of optical fibre tips--experiment and model.* Ultramicroscopy, 2000. **85**(4): p. 235.

54. Pangaribuan, T., et al., *Reproducible fabrication technique of nanometric tip diameter fiber probe for photon scanning tunneling microscope.* Jpn. J. Appi. Phys, 1992. **31**(9A Pt 2).

55. Xu, J., et al., *A novel temperature-insensitive optical fiber pressure sensor for harsh environments.* IEEE Photonics Technology Letters, 2005. **17**(4): p. 870-872.

56. Micron optics, I. *si720 Optical Sensing Analyzer*.

57. Belosludtsev, Y., et al., *DNA microarrays based on noncovalent oligonucleotide attachment and hybridization in two dimensions.* Analytical biochemistry, 2001. **292**(2): p. 250-256.

58. Lee, G., L. Chrisey, and R. Colton, *Direct measurement of the forces between complementary strands of DNA.* SCIENCE-NEW YORK THEN WASHINGTON-, 1994: p. 771-771.

59. Guo, Z., et al., *Direct fluorescence analysis of genetic polymorphisms by hybridization with oligonucleotide arrays on glass supports.* Nucleic Acids Research, 1994. **22**(24): p. 5456.

60. Tronin, A., et al., *Optimisation of IgG Langmuir film deposition for application as sensing elements.* Sensors and Actuators B: Chemical, 1996. **34**(1-3): p. 276-282.

61. Adsorption, E., *Assembly of multicomponent protein films by means of electrostatic layer-by-layer adsorption.* J. Am. Chem. Soc, 1995. **117**(22): p. 6117-6123.

62. Caruso, F., et al., *2. Assembly of alternating polyelectrolyte and protein multilayer films for*

immunosensing. Langmuir, 1997. **13**(13): p. 3427-3433.

63. Decher, G., *Fuzzy nanoassemblies: toward layered polymeric multicomposites.* Science, 1997. **277**(5330): p. 1232.

64. Decher, G., J. Hong, and J. Schmitt, *Buildup of ultrathin multilayer films by a self-assembly process: III. Consecutively alternating adsorption of anionic and cationic polyelectrolytes on charged surfaces.* Thin solid films, 1992. **210**: p. 831-835.

65. Hammond, P., *Recent explorations in electrostatic multilayer thin film assembly.* Current Opinion in Colloid & Interface Science, 1999. **4**(6): p. 430-442.

66. Decher, G. and J. Schmitt, *Fine-tuning of the film thickness of ultrathin multilayer films composed of consecutively alternating layers of anionic and cationic polyelectrolytes.* Trends in Colloid and Interface Science VI, 1992: p. 160-164.

67. Hao, E. and T. Lian, *Buildup of polymer/Au nanoparticle multilayer thin films based on hydrogen bonding.* Chem. Mater, 2000. **12**(11): p. 3392-3396.

68. Fang, M., et al., *A "Mix and Match" Ionic- Covalent Strategy for Self-Assembly of Inorganic Multilayer Films.* J. Am. Chem. Soc, 1997. **119**(50): p. 12184-12191.

69. Decher, G., et al., *New nanocomposite films for biosensors: layer-by-layer adsorbed films of polyelectrolytes, proteins or DNA.* Biosensors and Bioelectronics, 1994. **9**(9-10): p. 677-684.

70. Hong, J., et al., *Layer-by-layer deposited multilayer assemblies of polyelectrolytes and proteins: from ultrathin films to protein arrays.* Trends in Colloid and Interface Science VII: p. 98-102.

71. Lvov, Y., G. Decher, and G. Sukhorukov, *Assembly of thin films by means of successive deposition of alternate layers of DNA and poly (allylamine).* Macromolecules, 1993. **26**(20): p. 5396-5399.

72. Cassier, T., K. Lowack, and G. Decher, *Layer-by-layer assembled protein/polymer hybrid films: nanoconstruction via specific recognition.* Supramolecular Science, 1998. **5**(3-4): p. 309-315.

73. Lvov, Y., G. Decher, and H. Moehwald, *Assembly, structural characterization, and thermal behavior of layer-by-layer deposited ultrathin films of poly (vinyl sulfate) and poly (allylamine).* Langmuir, 1993. **9**(2): p. 481-486.

74. Iler, R., *The chemistry of silica: solubility, polymerization, colloid and surface properties, and biochemistry*. 1979: Wiley New York.

75. Halthur, T., P. Claesson, and U. Elofsson, *Stability of polypeptide multilayers as studied by in situ ellipsometry: Effects of drying and post-buildup changes in temperature and pH.* J. Am. Chem. Soc, 2004. **126**(51): p. 17009-17015.

76. Lowman, G. and S. Buratto, *Nanoscale morphology of polyelectrolyte self-assembled films probed by scanning force and near-field scanning optical microscopy.* Thin solid films, 2002. **405**(1-2): p. 135-140.

77. Lavalle, P., et al., *Comparison of the structure of polyelectrolyte multilayer films exhibiting a linear and an exponential growth regime: An in situ atomic force microscopy study.* Macromolecules, 2002. **35**(11): p. 4458-4465.

78. Bariain, C., et al., *Optical fiber humidity sensor based on a tapered fiber coated with agarose gel.* Sensors and Actuators B: Chemical, 2000. **69**(1-2): p. 127-131.

79. Yoo, D., S. Shiratori, and M. Rubner, *Controlling bilayer composition and surface wettability of*

sequentially adsorbed multilayers of weak polyelectrolytes. Macromolecules, 1998. **31**(13): p. 4309-4318.

80. Shiratori, S. and M. Rubner, *pH-dependent thickness behavior of sequentially adsorbed layers of weak polyelectrolytes.* Macromolecules, 2000. **33**(11): p. 4213-4219.

81. Michaels, A. and R. Miekka, *Polycation-polyanion complexes: Preparation and properties of poly-(vinylbenzyltrimethylammonium) poly-(styrenesulfonate).* The Journal of Physical Chemistry, 1961. **65**(10): p. 1765-1773.

82. Vermeer, A., F. Leermakers, and L. Koopal, *Adsorption of weak polyelectrolytes on surfaces with a variable charge. Self-consistent-field calculations.* Langmuir, 1997. **13**(16): p. 4413-4421.

83. Zhang, Y., *Miniature fiber-optic multicavity Fabry-Perot interferometric biosensor* in *Electrical and Computer Engineering* 2005, Virginia Polytechnic Institute and State University: Blacksburg, VA.

84. Wang, A., et al., *Molecular structure of a left-handed double helical DNA fragment at atomic resolution.* Nature, 1979. **282**: p. 680-686.

85. Elhadj, S., G. Singh, and R. Saraf, *Optical properties of an immobilized DNA monolayer from 255 to 700 nm.* Langmuir, 2004. **20**(13): p. 5539-5543.

86. Gray, D., et al., *Ellipsometric and interferometric characterization of DNA probes immobilized on a combinatorial array.* Langmuir, 1997. **13**(10): p. 2833-2842.

87. X. Shi, R.S., and F. Zhou, *Structural character multilayered DNA and polylysine composite films: influence of ionicof DNA solution on the extension of DNAincorporation.* Phys. Chem. B 2001. **106**: p. 1173-1180.

88. Wang, X., et al., *Label-free DNA sequence detection using oligonucleotide functionalized optical fiber.* Applied Physics Letters, 2006. **89**: p. 163901.

89. dos Santos Riccardi, C., et al., *Label-free DNA detection based on modified conducting polypyrrole films at microelectrodes.* Anal. Chem, 2006. **78**(4): p. 1139-1145.

90. Andrew, A., *Nanomedicine, Volume 1: Basic Capabilities*. Kybernetes, 2000. **29**(9/10): p. 509.

91. Rothemund, P., et al., *Design and characterization of programmable DNA nanotubes.* Journal of the American Chemical Society, 2004. **126**(50): p. 16344-16352.

92. Clark, H., et al., *Optical nanosensors for chemical analysis inside single living cells. 2. Sensors for pH and calcium and the intracellular application of PEBBLE sensors*. Anal. Chem, 1999. **71**(21): p. 4837-4843.

93. Cavalcanti, A., et al., *Medical nanorobot architecture based on nanobioelectronics.* Recent Patents on Nanotechnology, 2007. **1**(1): p. 1-10.